2D Edge-based Finite Elements for Guided and Scattered Wave Problems

Riana Helena Hansmann

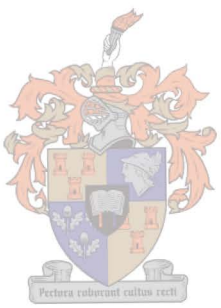

Thesis presented in partial fulfilment of the requirements
of the degree Master of Science in Engineering
at the University of Stellenbosch

March 1999

Supervisor: Prof. D. B. Davidson

Stellenbosch University https://scholar.sun.ac.za

Declaration

I, the undersigned, hereby declare that the work contained in this thesis is my own, unless stated otherwise and has not previously been submitted at any university for a degree.

11/02/99
Date

Stellenbosch University https://scholar.sun.ac.za

Abstract

This thesis may be divided into two parts: the first describes the Finite Element Method (FEM) and its application to guided wave problems. The second part is devoted to scattering configurations, specifically the use of the Boundary Element Method (BEM) and the hybrid Finite Element Method-Boundary Element Method (FEM-BEM) to obtain solutions for scattering problems. The formulations are restricted to two dimensions throughout the thesis.

A variational formulation is introduced and the implementation of boundary conditions is described. The use of vector approximation functions for the Finite Element Method is explained and the advantages highlighted. The properties of these functions are derived and graphical representations are given. A comparison between a lower order and higher order approximation is made. This is applied to problems which demonstrate the capabilities of the Finite Element Method such as ridged waveguides and circular waveguides containing eccentric dielectric rods. Results obtained compare well to analytic solutions, in the cases where these are available.

An integral equation for scattering problems is derived. This relates the tangential field components on a contour enclosing a scattering object to the scattered fields and enables a solution to be obtained when the tangential components on the contour are known. It is shown how the interior region enclosed by the contour is discretised and how the Finite Element Method can be coupled with the Boundary Element Method by imposing continuity conditions on the enclosing contour. The resulting system of equations obtained may be solved. Solutions for scattering from perfectly conducting cylinders are obtained and compare well to analytic results.

Stellenbosch University https://scholar.sun.ac.za

Opsomming

Hierdie tesis bestaan uit twee dele: die eerste beskryf die toepassing van die Eindige Element Metode (EEM) vir golfleier probleme. Die tweede deel handel oor strooiings probleme en die toepassing van die hibriede Eindige Element-Randelement Metode om numeriese oplossings vir hierdie tipe probleme te vind. Die formulerings in hierdie tesis is deurgaans tweedimensioneel van aard.

'n Variasionele formulering word beskryf saam met die geassosieerde randvoorwaardes. Die gebruik van vektor basis funksies vir die Eindige Element Metode word beskryf en die voordele uitgelig. Die eienskappe van hierdie vektor funksies word grafies voorgestel en herlei. Verskillende orde benaderings is geïmplimenteer en die akkuraatheid van die benaderings word ondersoek. Probleme wat die vermoë van die metode ten toon stel is gekies, byvoorbeeld golfleiers met riwwe en ronde golfleiers wat diëlektriese silinders bevat. In die gevalle waar analitiese oplossing beskikbaar is, vergelyk die Eindige Element resultate goed met die analitiese oplossings.

In die tweede deel van die tesis word 'n integraal vergelyking wat van toepassing is op strooiingsprobleme, afgelei. Die tangensiale veld-komponente op 'n kontoer wat 'n voorwerp omsluit word in verband gebring met die verstrooide veldkomponente elders in die omgewing rondom die voorwerp. Die diskretisasie van die omsluite gebied en die koppeling van die Eindige Element Metode met die Rand-Element Metode deur kontinuïteitsvoorwaardes op die kontoer word bespreek. 'n Stelsel van vergelykings word gevorm wat opgelos kan word om die veldkomponente op die kontoer en sodoende die strooiingseffek van 'n voorwerp te bepaal. Die strooiingseffek van perfek geleidende silinders is bepaal en vergelyk goed met analitiese oplossings.

Stellenbosch University https://scholar.sun.ac.za

Acknowledgements

I would like to thank the following people who made a contribution to my thesis:

My supervisor, Prof. Davidson, whose guidance and enthusiasm I appreciate.

Dr. Isak Theron and Francois Rabie from the Penthouse for assistance in mastering the intricacies of LaTeX.

Melanie Botha who read this document while still in its intermediate stages and provided valuable suggestions and corrections.

My husband, Mark, and my parents for their support.

Stellenbosch University https://scholar.sun.ac.za

Keywords

Finite Element Method (FEM)
Edge-based Finite Elements
Vector basis functions
hierarchical basis functions
interpolatory basis functions
Hybrid Finite Element-Boundary Element Method (FEM-BEM)

Stellenbosch University https://scholar.sun.ac.za

List of Notation

$\mathbf{A}$	vector
$\overline{\overline{A}}$	dyadic
$[A]$	matrix
$[A]_{m,n}$	matrix entry (m,n) of matrix A
λ_i	simplex coordinate with unit value at simplex vertex i
$\mathbf{r}$	position vector assosiated with observation point
$\mathbf{r}'$	position vector assosiated with source point
$\hat{m}$	unit normal vector to 2D surface
$\hat{n}$	unit normal vector to 3D surface
$G_0(\mathbf{r}, \mathbf{r}')$	free space Green's function, (2D in this thesis)

Stellenbosch University https://scholar.sun.ac.za

Contents

Stellenbosch University https://scholar.sun.ac.za

Stellenbosch University https://scholar.sun.ac.za

List of Figures

Stellenbosch University https://scholar.sun.ac.za

Stellenbosch University https://scholar.sun.ac.za

Stellenbosch University https://scholar.sun.ac.za

List of Tables

Stellenbosch University https://scholar.sun.ac.za

Introduction and Overview of this Thesis

The phenomenon of electromagnetic wave propagation, from visible light to radio waves, has fascinated many over the past few centuries. With the concepts of wave propagation understood the focus now is the practical application of it to antenna design, military applications and many more applications which become possible. The design engineer needs a solid foundation in electromagnetics and good modelling tools. Here is the opportunity for those who enjoy the challenges of numerical modelling of electromagnetic wave propagation as accurately and as effectively as possible in terms of computational times. Many techniques exist to model the behaviour described by Maxwell's equations. Some of these are approximate techniques which are valid for high frequencies, while others such as integral equation methods are exact, but computationally intensive. Paging through relevant periodicals, it is clear these numerical methods are an active region of research and many contributions, of which many are applications, are published every month.

The Finite Element method is a differential equation technique and is well suited to the modelling of inhomogeneous structures with complex geometries. It involves the discretisation of the entire volume (in three dimensional modelling). The matrices involved are usually sparse and special storage schemes exist which save memory space and allow large matrices to be handled with relative ease. Techniques to solve sparse matrix systems reduce the computational time associated with these problems. However, infinite problem domains cannot be handled with this technique without termination of the region by the use of absorbing boundary conditions or some other form of termination. The Finite Element Method for guided wave configurations is applied effectively to analyse and design waveguide structures. Examples of these are filters and increased-bandwidth waveguides; for example, ridged waveguides. Another application is the analysis of dielectric loaded cavities.

The Boundary Element Method is an integral equation method and allows infinite domains to be considered. The formulation is exact (the implementation is not exact, since the solution is approximated with basis functions which are genrally of low order) and is equally valid for far field solutions and near field solutions. It requires discretisation of a surface enclosing a volume (3D) and incorporates the Sommerfeld radiation condition into the formulation, which means that any solution obtained will satisfy this requirement. Unfortunately, densely populated matrices are generated and an huge amount of memory space is required to solve problems large in terms of wavelengths.

The hybrid Finite Element-Boundary Element Method (FEM-BEM) is the combination of both methods, exploiting the advantages of each in the region where it is most appro-

Stellenbosch University https://scholar.sun.ac.za

priately used. The FEM-BEM is often used for antenna design, for example cavity backed antenna arrays and the analysis of infinite periodic arrays. It is also applied to determine the radar scattering effect of structures. Very relevant today is the modelling of the effect of radiation on the human body, which can be investigated by the use of this method. The characterisation of the scattering effect of materials and propagation environments is another possibility. A restrictions of the technique is the electromagnetic size of the configuration considered, since at least a tenth of a wavelength discretisation is required to obtain accurate results.

The subject of this thesis is the investigation of the details of the implementation of the Finite Element Method (FEM) and finally the hybrid Finite Element-Boundary Element Method (FEM-BEM) as applied to respectively guided wave and scattering problems. All the work presented was restricted to two dimensional geometries. This simplifies the discretisation of the configurations and focuses the attention on the technique itself.

Chapter 1 briefly introduces the reader to the FEM technique. The minimisation of a functional that corresponds to the solution of a boundary value problem is presented. Boundary conditions and discretisation details are mentioned. Chapter 2 is a summary of the literature on vector based finite elements, describing the most recent developments. It is shown that various possibilities exist in the case of the basis functions, which determine the accuracy and reliability of the results. A motivation for the use of vector basis sets is given. In chapter 3 a hierarchical basis set is chosen from the options available and the element matrices are derived for the two-dimensional case. The properties of the approximations as derived from the basis set implemented are explained. An interesting property, which is characteristic of the basis set chosen, is the different orders of approximation used for normal and tangential components on boundaries. This is derived and illustrated. Higher order approximations are also examined. It is explained how the TE and TM modes are found and whether the E or H field is discretised to obtain the desired modes. The application of the theory in chapters 1 to 3 for guided wave structures is presented in chapter 4. Examples are chosen that demonstrate the capabilities of the Finite Element method when a vector basis set is implemented.

The rest of the thesis describes scattering problems. Chapter 5 contains the derivation in the two dimensional case of the scattering equations. Huygens' principle is the starting point for the discretisation and setting up of matrix equations. The derivations are specifically two dimensional and it is based on the three dimensional derivations found in the literature. Chapter 6 presents results obtained for scattering configurations for which analytic solutions are available. This chapter is followed by a general overview of the thesis and comments on the results which were obtained.

Stellenbosch University https://scholar.sun.ac.za

Chapter 1

Introduction to the FEM method

1.1 Introduction

This chapter serves as a general introduction to the basics of the Finite Element method. It is an overview of the method and aims to highlight the most important concepts. The book by Silvester and Ferrari [1] is both an excellent introductory text, and a source of much more detailed information. Jin [2] contains a chapter on variational principles for electromagnetics and [1] also contains more detail on some of the topics presented in this chapter. A familiarity with simplex elements and coordinates is assumed in this chapter. The basics of these elements are explained in appendix A.

1.2 Formulation

The FEM method is traditionally based on the minimum energy principle. This is equivalent to minimisation of the energy functional [3]

$$F(\mathbf{U}) = \frac{1}{2}\iint_{\Omega}(\frac{1}{p}(\nabla \times \mathbf{U}) \cdot (\nabla \times \mathbf{U}) - k_0^2 q\mathbf{U} \cdot \mathbf{U})dS \tag{1.1}$$

where $\mathbf{U}$ may be the $\mathbf{E}$ or $\mathbf{H}$ field, while p and q are the material parameters in the region under consideration. If $\mathbf{U}$ represent the E -field vector, then $p = \mu_r$ and $q = \epsilon_r$. Similarly, if $\mathbf{U}$ represents the H-field vector, $p = \epsilon_r$ and $q = \mu_r$.

It can be shown that the solution to the differential equation

$$\mathcal{L}\mathbf{U} = f \tag{1.2}$$

associated with a boundary-value problem can be obtained by minimisation of the associated energy functional [2]. In this case the differential equation is the vector Helmholtz equation

$$\nabla \times \frac{1}{p}\nabla \times \mathbf{U} - k_0^2 q\mathbf{U} = 0 \tag{1.3}$$

Certain requirements for the differential operator $\mathcal{L}$ must be met.

Jin [2] proves that the differential equation results from the functional F when the first variation is zero. He then proves that the minimum of the functional F corresponds to the point where the first variation is zero.

Stellenbosch University https://scholar.sun.ac.za

The finite element method divides the problem domain into elements, where basis functions are used to approximate the field variable over each element. The discretised energy functional is now minimised. In this case, simplex elements are used. A simplex element in 1D is a line segment, in 2D it is a triangle and a tetrahedron in 3D. Attention will be restricted to triangular elements (2D simplexes).

U is approximated inside every element as

$$\mathbf{U}_{element} = \sum_{k=1}^{n} \mathbf{w}_k(\mathbf{r}) u_k \tag{1.4}$$

for a vector formulation. The basis function ($\mathbf{w}_k$), is a vector function of position $\mathbf{r}$ in the element. u_k is an edge coefficient in this case.

However, for a scalar formulation, the field variable may be expressed as a function of the variable's value at each of the n nodes on an element (which are not necessarily only the three vertex points)

$$U_{element} = \sum_{k=1}^{n} w_k u_k \tag{1.5}$$

Here u_k is the nodal coefficient at node k. Note that in this case the basis function is a scalar function. The first type of expansion as presented in equation (1.4) will be used. This is a more recent development than nodal expansions. Nodal based FEM were previously employed for both structural engineering and electromagnetic problems. At this stage mostly vector formulations are in use by the electromagnetics community. It is also possible to implement both vector and scalar basis functions in the same problem [4], although this will not be described in this thesis.

1.3 Discretisation and Boundary Conditions

1.3.1 Discretisation of the Functional

The discretised functional is

$$F(\mathbf{U}) = \frac{1}{2}([U]^t[S][U] - k^2[U]^t[T][U]) \tag{1.6}$$

$[U]$ is the unknown coefficient matrix of the discretised field variable. Every element is numbered and every edge is assigned an edge number, which corresponds to the unknown coefficient with the same index. These coefficients are all contained in the coefficient matrix. The matrices S and T are included in (1.6). These are referred to as element matrices, where a distinction is made between global element matrices and element matrices for single elements. The latter is indicated with the superscript e, to indicate that only one element is considered. The global element matrices are found by combining the effect of every individual matrix. This must be done since (1.6) requires matrices containing contributions from all the elements.

Stellenbosch University https://scholar.sun.ac.za

To obtain an equation enabling one to solve for the unknown field variable, minimisation with respect to each edge coefficient in turn must be done. This leads to

$$[S][U] - k^2[T][U] = 0 \tag{1.7}$$

Here $[S]$ and $[T]$ are global matrices. Now $[S]^e$ and $[T]^e$ (for a single element) must first be found:

$$[S]^e_{ij} = \iint_\Omega \frac{1}{p}(\nabla \times \mathbf{w}_i) \cdot (\nabla \times \mathbf{w}_j) d\Omega \tag{1.8}$$

$$[T]^e_{ij} = \iint_\Omega q\mathbf{w}_i \cdot \mathbf{w}_j d\Omega \tag{1.9}$$

$\mathbf{w}_i$ and $\mathbf{w}_j$ are the i-th and j- th basis functions defined on element e and Ω is the area of the element (2D) or the volume of the element (3D).

Tables with [S] and [T] matrices for 3D CT/LN [1] are listed by Lee and Mittra [3] while Jin [2] does the same for the 2D case (CT/LN).

Now the global [S] and [T] matrices are found from the individual element matrices; this process is referred to as **assembly**. It amounts to adding the energy contributions from every element and is described in Silvester and Ferrari [1]. Integration is performed over every element. Useful integration formulae for simplex integrals are given by Jin [2, p. 82].

1.3.2 Boundary Conditions

The boundary conditions that will be encountered are Dirichlet (essential): $\mathbf{U} \times \hat{n} = 0$ or Neumann : $\hat{n} \cdot \nabla \times \mathbf{U} = v_0$.

The boundary conditions are specified with the boundary value problem that is to be solved.

1.3.3 Natural and Essential Boundary Conditions and Natural Continuity Conditions

Previously it was mentioned that the first variation of the functional is set to zero. This results in a boundary integral forced to zero [1]. There are three possibilities. The boundary integral is over a boundary where either the essential or natural boundary conditions are required, or the boundary is between two adjacent elements which may also have different material parameters.

Let the approximation to the solution be $\mathbf{U}$ and $\mathbf{u}$ the correct solution. When the tangential components of the correct solution are known, the boundary integral is zero. This is

$$\hat{n} \times \mathbf{U} = \hat{n} \times \mathbf{u} \tag{1.10}$$

If the essential boundary conditions are not specified, the natural boundary condition

$$\hat{n} \cdot \nabla \times \mathbf{u} = 0 \tag{1.11}$$

[1] constant tangential, linear normal components on boundaries, these are the lowest order basis functions

Stellenbosch University https://scholar.sun.ac.za

is forced by the fact that the first variation is set to zero [1].

The third possibility is that the boundary is an inter-element boundary. On inter-element boundaries there is no contribution to the first variation, which ensures that the solution obtained is not dependent on the discretisation. Silvester and Ferrari [1] also show that tangential continuity on inter- element boundaries is the only requirement to ensure that the first variation of the functional is zero. This also holds when material discontinuities occur. In the case where adjacent elements have identical material parameters, the normal components are continuous; this is referred to as a natural continuity condition.

Tangential continuity between elements is enforced by equating coefficients of adjacent edge basis functions. Normal continuity is not enforced. Adjacent edges are often numbered in the opposite direction e.g. edge (i,j) and edge(j,i) , which may require that coefficients of the adjacent oppositely directed elements must be equal in magnitude, but different in sign. However, this is dependent on the form of the basis function and due to the vector nature of the basis functions.

Silvester and Ferrrari [1] use a connection matrix idea to explain how the nodal continuity is established. This is done in the same way for edge continuity. It is in fact what is implicitly done when element matrices are connected, but the matrix multiplication is much too time consuming to be effective. For this reason the effect of the connection matrix is explained here and in the code the elements of the connected matrix are simply inserted into the correct positions.

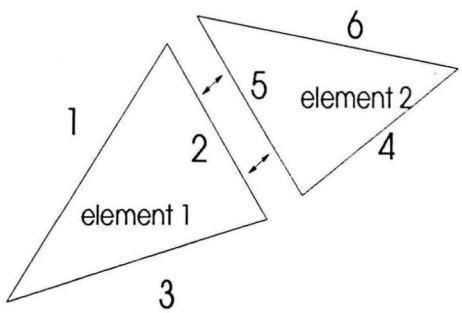

Figure 1.1: Connection of two disconnected elements where 3 basis functions are defined on an element. The numbers indicated represent the edge numbers.

Consider two disconnected elements numbered as shown in figure 1.1. Here we have the disconnected coefficients numbered 1 to 6. The triangle edges are numbered 1 2 3 and 6 4 5 where edges 2 and 5 must be connected.

The disconnected coefficient matrix from (1.6) is now

$$\begin{bmatrix} u_1 \\ u_2 \\ u_3 \\ u_4 \\ u_5 \\ u_6 \end{bmatrix} \tag{1.12}$$

(note that the order of numbering is arbitrary) and the associated disconnected element matrix S (for CT/LN or 3 degrees of freedom) as an illustration

Stellenbosch University https://scholar.sun.ac.za

$$S_{dis} = \begin{bmatrix} s_{11} & s_{12} & s_{13} & 0 & 0 & 0 \\ s_{21} & s_{22} & s_{23} & 0 & 0 & 0 \\ s_{31} & s_{32} & s_{33} & 0 & 0 & 0 \\ 0 & 0 & 0 & s_{44} & s_{45} & s_{46} \\ 0 & 0 & 0 & s_{54} & s_{55} & s_{56} \\ 0 & 0 & 0 & s_{64} & s_{65} & s_{66} \end{bmatrix} \tag{1.13}$$

Now note that the coefficients 2 and 5 should be equal in magnitude, possibly opposite in sign if edges 2 and 5 are oppositely directed. The connection matrix C relates the connected and disconnected coefficient vectors and eliminates the identical coefficients

$$U_{dis} = CU_{con} \tag{1.14}$$

where U_{con} is now the coefficient matrix containing each edge coefficient only once. For the example in figure 1.1 the expression (1.14) is

$$\begin{bmatrix} u_1 \\ u_2 \\ u_3 \\ u_4 \\ u_5 \\ u_6 \end{bmatrix} = \begin{bmatrix} 1 & 0 & 0 & 0 & 0 \\ 0 & 1 & 0 & 0 & 0 \\ 0 & 0 & 1 & 0 & 0 \\ 0 & 0 & 0 & 1 & 0 \\ 0 & 1 & 0 & 0 & 0 \\ 0 & 0 & 0 & 0 & 1 \end{bmatrix} \begin{bmatrix} u_1 \\ u_2 \\ u_3 \\ u_4 \\ u_6 \end{bmatrix} \tag{1.15}$$

The connection matrix now leads to smaller global element matrices S and T

$$\begin{aligned} S_{con} &= C' S_{dis} C \\ T_{con} &= C' T_{dis} C \end{aligned} \tag{1.16}$$

Then the connected element S matrix is now

$$S_{con} = \begin{bmatrix} s_{11} & s12 & s13 & 0 & 0 \\ s21 & s22 + s55 & s23 & \pm s54 & \pm s56 \\ s31 & s32 & s33 & 0 & 0 \\ 0 & \pm s45 & 0 & s44 & s46 \\ 0 & \pm s65 & 0 & s64 & s66 \end{bmatrix} \tag{1.17}$$

The same holds for the T matrix (1.9). The sign in the indicated positions depends on whether the edges are numbered in the same or in the opposite directions and the form of the basis functions. These will be discussed in the next chapter, but it will become clear that

$$\mathbf{w}_{ij}^{(0.5)} = -\mathbf{w}_{ji}^{(0.5)} \tag{1.18}$$

$$\mathbf{w}_{ij}^{(1)} = \mathbf{w}_{ji}^{(1)} \tag{1.19}$$

for the half and first order basis functions, whose form is shown later.

Stellenbosch University https://scholar.sun.ac.za

1.4 Various Basis Functions

It has already been shown that one has a choice between a scalar approximation or a vector formulation. The choice depends on whether the problem considered can be reduced to a scalar problem (2D configurations or 3D with one of the object dimensions infinite) or whether it is more conveniently expressed as a vector problem. The manifestation of spurious modes associated with the choice is also important. Spurious modes are modes which satisfy the boundary conditions but are not valid solutions of the wave equation. These are obtained along with the valid solutions and are difficult to identify when a scalar formulation is used, since their wavenumbers are similar to the correct ones. The vector formulation results in zero or very small wavenumbers for spurious modes, enabling easy identification of these.

When vector basis functions are considered, the two options are **hierarchical** or **interpolatory** functions. (It is possible to use functions which are neither hierarchical nor interpolatory e.g. as in [5])

Finite elements are hierarchical when each lower order basis set is a subset of the basis set for any higher order set [4]. The advantage of using hierarchical functions is that the order of approximation is easily increased by simply adding more (higher order) functions. The interpolatory basis functions have the advantage of lower element matrix condition numbers than hierarchical basis functions [6], which informally speaking is a measure of the degree of ill- posedness of the element matrices.

1.5 Conclusion

The finite element method was described, along with the important concepts that will be used in the remainder of the thesis. The FEM can be summarised as: a discretisation of the domain with the associated basis functions; the minimisation of the functional, bearing in mind the boundary conditions; and finally the solution of the matrix equation that resulted from this process. The vector basis sets were chosen even though it is possible to formulate the two dimensional problems as a scalar problem. In this thesis the vector basis sets are specifically implemented to investigate their properties in the two dimensional case, where the geometry is reasonably simple and the Finite Element mesh easily visualised.

Stellenbosch University https://scholar.sun.ac.za

Chapter 2

Literature Survey : Vector Basis Functions

2.1 Introduction

The aim of this chapter is to expose the basic ideas available in the literature and to follow the development of this field over the past few years. It is interesting that not all of the ideas entertained by researchers were correct. One of the most interesting concepts associated with these basis functions is the possibility that spurious modes could be introduced, should it be implemented incorrectly. The various possible options found in the literature will be compared with the properties listed. A detailed description of the derivation of these properties for the basis set used by the author will be delayed until the next chapter.

2.2 Spurious modes

The following definitions are used frequently throughout the literature.

Definition 2.1 *The edge element space is the set of all possible fields that can be expressed as a linear combination of the edge basis functions associated with the edges of the mesh.*

$$E = \{\mathbf{E} \mid \mathbf{E} = \sum_{i=1}^{M} e_i w_i(x, y)\} \tag{2.1}$$

M is the number of edges in the mesh.

Definition 2.2 *The curl null space is* $G = \{\mathbf{E} \mid \mathbf{E} \in E \text{ and } \nabla \times \mathbf{E} = 0 \text{ in } \Omega\}$

Spurious modes are modes which are non-physical, i.e. they cannot exist. However, these modes are valid solutions to the vector Helmholtz equation, but do not satisfy all of the Maxwell equations [9]. In [7] the origin of spurious modes in both the scalar case and for vector basis functions is examined. This article explains parts of the material discussed by Nedelec, which is unfortunately not easily understood by non-mathematicians. It is stated that spurious modes are "badly formed static solutions" which means basically that spurious

UNIVERSITEITSBIBLIOTEEK

Stellenbosch University https://scholar.sun.ac.za

	2D (triangle)	3D (tetrahedron)
edge	$3k$	$6k$
face	$k(k-1)$	$4k(k-1)$
entire domain	-	$\frac{k(k-1)(k-2)}{2}$
total	$k(k+2)$	$\frac{k(k+2)(k+3)}{2}$

Table 2.1: Number of degrees of freedom for order $H_k(\text{curl})$.

solutions are of the form $\nabla\phi$ with ϕ a scalar function. An interesting comment here is that spurious solutions, being static solutions, do not propagate and thus do not affect the validity of far-field solutions.

In earlier papers it is often stated that divergence free bases are required for non spurious modes [8, p. 12]. This notion became very popular and was widely accepted for a while before it was exposed as a mistake [7] and [9].

The approximation should be such that the curl of the approximation contains all of the terms in the curl range space of p- th order, for a p- th order of convergence to be established.

Note that the number of terms in a complete polynomial of order p is $0.5(p+1)(p+2)$. This is also referred to as its dimension. Now the edge space E, defined above, is referred to as $H^p(curl)$, with p the highest order of complete polynomial in the range space of the curl operator. The dimension of $H^p(curl)$ is the sum of the dimensions of the curl range space and the curl null space. Spurious modes are caused by either (1) an incomplete polynomial function in the null space of the curl operator or (2) a linear dependence existing among the basis functions [10].

Nedelec [11] set down constraints for approximations in terms of basis sets that would result in optimal basis functions with correct null space modelling, ensuring that all spurious modes have zero eigenvalues.

2.3 The Advantages of Edge-based Functions

The edge- based vector functions identify very clearly the tangential components of the fields and provide tangential continuity by simply equating edge coefficients, as was shown in chapter 1. The tangential and normal components are clearly separable. In the case of nodal based functions, the tangential and normal components are both forced to be continuous. On material interfaces, the normal component of the field vector is physically required to be discontinuous, and this can only be modelled correctly with the use of the vector basis functions, where normal continuity is not imposed. The edge- based function also provides better modelling at sharp corners, where singularities are found and the field changes direction rapidly. The properties of edge- based functions results in better spurious mode modelling, in fact all the spurious modes are associated with zero eigenvalues and are now easily identified.

Stellenbosch University https://scholar.sun.ac.za

Table 2.2: Comparison between the various basis functions suggested in the literature.

	Webb	March '94 :Peterson (2D)	June '96 :Savage and Peterson	March '98 :Savage
$H_0(\text{curl})$	1-6: $\lambda_i\nabla\lambda_j - \lambda_j\nabla\lambda_i$	1-6: $\lambda_i\nabla\lambda_j - \lambda_j\nabla\lambda_i$	1-3: $\lambda_i\nabla\lambda_j - \lambda_j\nabla\lambda_i$	1-6: $\lambda_i\nabla\lambda_j - \lambda_j\nabla\lambda_i$
Linear	7-12:$\lambda_i\nabla\lambda_j + \lambda_j\nabla\lambda_i$	-	-	-
$H_1(\text{curl})$	8 face functions: 13-16: $\lambda_k\lambda_j\nabla\lambda_i$ 17-20: $\lambda_k\lambda_i\nabla\lambda_j$	1-6: $\lambda_i\nabla\lambda_j \quad i \neq j;$ 7: $\lambda_2\lambda_3\nabla\lambda_1 - \lambda_1\lambda_2\nabla\lambda_3$ 8: $\lambda_1\lambda_3\nabla\lambda_2 - \lambda_1\lambda_2\nabla\lambda_3$	1-12: $\lambda_i\nabla\lambda_j \quad i \neq j;$ 8 face functions: $\lambda_i\lambda_j\nabla_k - \lambda_i\lambda_k\nabla_j \quad i < j < k$ $\lambda_i\lambda_j\nabla_k - \lambda_i\lambda_k\nabla_j \quad i < j < k$	1-6: $\lambda_i\nabla\lambda_j - \lambda_j\nabla\lambda_i$ 7-12: $\lambda_i\nabla\lambda_j + \lambda_j\nabla\lambda_i$ 8 face functions as before

Stellenbosch University https://scholar.sun.ac.za

2.4 Degrees of Freedom and the Assignment of These to Element Edges and Faces

A finite element has associated with it degrees of freedom which have been defined by Nedelec [11]. These are associated with edges, faces and the entire domain of the finite element. The number of these are basically the number of unknowns for an element and are explained in table 2.1.

2.4.1 Hierarchical Functions

Table 2.2 summarises the subtle differences of basis functions as implemented by various workers. It is clear that the $H_0(\text{curl})$ basis functions are always of the form given, in fact, even in the interpolatory case (see [6]) these basis functions are incorporated into the basis sets. Webb [12] proposed a hierarchical basis set which is compared to the scalar basis functions in his article. This is the only case where the linear hierarchical basis functions are suggested. Peterson [9] works in 2D and presents the 2D basis sets, but these are not hierarchical. Savage and Peterson [5] later extended this work to 3D and presented higher order basis sets up to order $H_2(\text{curl})$. The most recent addition is by Savage [6], who shows fully hierarchical basis sets up to order $H_3(\text{curl})$ and also for comparison gives the interpolatory basis sets up to order $H_3(\text{curl})$. Element matrix derivations of $H_0(\text{curl})$ (3D) may be found in [3] and 2D in [2]. $H_1(\text{curl})$ element matrices for the basis set in table 2.2 (Savage and Peterson) are given in [5]. Note that the $H_0(\text{curl})$ basis functions are also referred to as CT/LN (constant tangential- linear normal components on element edges) basis functions and the $H_1(\text{curl})$ basis functions are referred to as LT/QN (linear tangential-quadratic normal components on element edges) basis functions. This will be explained in chapter 3.

A less standard assignment of degrees of freedom was done in [13] as shown in figure 2.1. Here the third edge in the centre of the element is expressed in terms of the other two, since the three edge functions inside the element cannot be linearly independent. However, [13] does not show how the degrees of freedom would be assigned for higher order approximations. The degrees of freedom are $k(k+2)$, which is as shown in table 2.1.

2.4.2 Interpolatory Functions

While Webb [12] proposed the scheme of hierarchical basis functions, it is also possible to derive interpolatory vector functions in a similar manner as was done in the scalar case. The same interpolation functions [1] $R_i(p,\lambda)$ are used again, $R_i(p,\lambda)$ has i zeros spaced $1/p$ apart, from zero to $\frac{i-1}{p}$.

$$R_i(n,\lambda) = \prod_{k=0}^{i-1} \frac{\lambda - k/n}{i/n - k/n} \tag{2.2}$$

Shifted interpolation functions are also defined

Stellenbosch University https://scholar.sun.ac.za

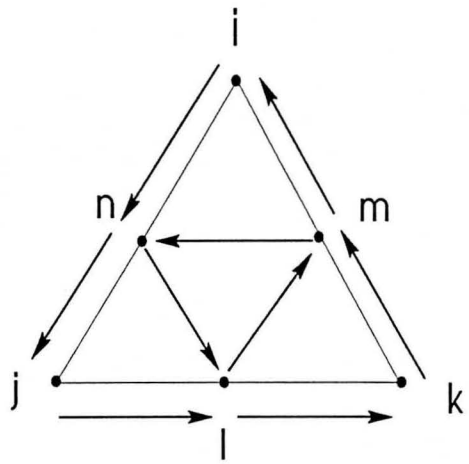

Figure 2.1: Assignment of degrees of freedom in [13].

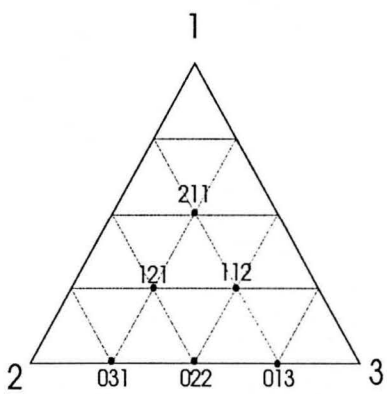

Figure 2.2: Interpolation nodes for first set of basis functions.

$$\begin{aligned} \hat{R}_i(p,\lambda) &= R_{i-1}(p,\lambda - 1/p) \\ &= \begin{cases} \frac{1}{(i-1)!}\prod_{k=1}^{i-1}(p\lambda - k), & 2 \leq i \leq p+1 \\ 1, & i = 1 \end{cases} \end{aligned} \tag{2.3}$$

This modified or shifted polynomial has no zero at $\lambda = 0$, which is a useful property of which the importance will become evident later.

The basic approach is to take the product between the usual $H_0(curl)$ (table 2.2) vector basis function and a scalar p-th order polynomial; specifically the product of a standard interpolation function (referred to as a Silvester polynomial) and two modified functions is used to form the basis functions.

The set of basis functions are then given in [14] as

Stellenbosch University https://scholar.sun.ac.za

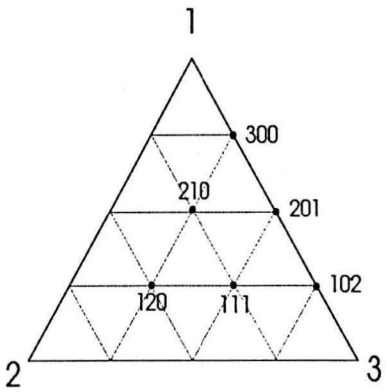

Figure 2.3: Interpolation nodes for second set of basis functions.

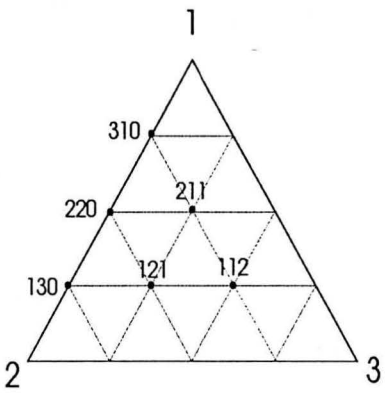

Figure 2.4: Interpolation nodes for third set of basis functions.

$$\begin{aligned}
\mathbf{\Omega}^1_{ijk}(\mathbf{r}) &= N^1_{ijk} R_i(p+2,\lambda_1)\hat{R}_j(p+2,\lambda_2)\hat{R}_k(p+2,\lambda_3)\mathbf{\Omega}_1(\mathbf{r}) \\
&\qquad i=0,1,...,p \quad j,k=1,2,...,p+1 \\
\mathbf{\Omega}^2_{ijk}(\mathbf{r}) &= N^2_{ijk} R_i(p+2,\lambda_1)\hat{R}_j(p+2,\lambda_2)\hat{R}_k(p+2,\lambda_3)\mathbf{\Omega}_2(\mathbf{r}) \\
&\qquad i=0,1,...,p \quad j,k=1,2,...,p+1 \\
\mathbf{\Omega}^3_{ijk}(\mathbf{r}) &= N^1_{ijk} R_i(p+2,\lambda_1)\hat{R}_j(p+2,\lambda_2)\hat{R}_k(p+2,\lambda_3)\mathbf{\Omega}_3(\mathbf{r}) \\
&\qquad i=0,1,...,p \quad j,k=1,2,...,p+1
\end{aligned} \tag{2.4}$$

where $i+j+k=p+2$.

This is illustrated for the case where $p=2$ in figures 2.2, 2.3 and 2.4. Interpolation nodes occur only on one of the edges. This is due to the fact that only the standard interpolation function has a zero at $\lambda = 0$, while the two modified functions do not have this zero. Each of the general forms of the basis functions above lead to 6 basis functions, where each one of these interpolates at one of the nodes shown in the above figures. The numbering indicates the indices i, j, and k, which correspond to the functions in 2.4. To eliminate linear dependencies of the basis functions, only two of the three basis functions which are interpolatory at each interior point are retained.

The degrees of freedom are the same number as before i.e. $(p+1)(p+3)$ as in the hierarchical case.

Stellenbosch University https://scholar.sun.ac.za

In the same manner it is shown in [14] how to define these interpolation functions on tetrahedrons and brick elements. Full expressions for these are given in [14] for first to third order approximations.

2.5 Conclusion

All the possible options may leave the reader confused as to which basis set is the best to use. An interesting question is whether a variation on the above basis sets or something entirely new could not perhaps provide better performance. Required for any basis set is linear independence, and preferably adherence to Nedelec's constraints, which will assure proper null space modelling. Certainly Nedelec's [11, 15] publications were the foundation for most of the further work by engineers.

Stellenbosch University https://scholar.sun.ac.za

Chapter 3

Hierarchical Basis Functions

3.1 Introduction

In the previous chapter the properties of hierarchical basis functions were discussed. The difference between interpolatory and hierarchial basis functions was also explained. This chapter will focus on hierarchical vector basis functions. The properties will be investigated and the advantages of the structure highlighted.

3.2 Properties

The field variable at any point inside or on the element boundaries is expressed as the combined effect of every basis function used for the specific element. The vector basis function is highly suited to enforce the required tangential continuity between elements in a very natural manner. Tangential components between elements are made continuous, while continuity is not imposed on the normal components explicitly, allowing them to be discontinuous at inhomogenous boundaries.

Consider a 2D linear complete vector function

$$\mathbf{M} = \hat{\mathbf{x}}[A + Bx + Cy] + \hat{\mathbf{y}}[D + Ex + Fy] \tag{3.1}$$

Here the degrees of freedom are the six unknowns, A,B,C,D,E and F. Nedelec proposed constraints to reduce the degrees of freedom, by determining which actually contribute to non-spurious modes. The constraints in two dimensions are:

$$\frac{\partial \mathbf{M}_x}{\partial x} = 0 \tag{3.2}$$

$$\frac{\partial \mathbf{M}_y}{\partial y} = 0 \tag{3.3}$$

$$\frac{\partial \mathbf{M_x}}{\partial y} + \frac{\partial \mathbf{M_y}}{\partial x} = 0 \tag{3.4}$$

Stellenbosch University https://scholar.sun.ac.za

Order	Basis functions	
CT/LN	$\overline{w}_k = \lambda_i \nabla\lambda_j - \lambda_j \nabla\lambda_i$	$k = 1,2,3$
LT/QN	$\overline{w}_k = \begin{cases} \lambda_i \nabla\lambda_j - \lambda_j \nabla\lambda_i & k = 1,2,3 \\ \lambda_i \nabla\lambda_j + \lambda_j \nabla\lambda_i & k = 4,5,6 \\ (\nabla\lambda_i)\lambda_j\lambda_k & k = 7 \\ (\nabla\lambda_j)\lambda_i\lambda_k & k = 8 \end{cases}$	

Table 3.1: Hierarchical basis functions.

These reduce the number of constraints to three :

$$\mathbf{M}' = \hat{\mathbf{x}}[A + Cy] + \hat{\mathbf{y}}[D - Cx] \tag{3.5}$$

Consider the vector wave equation for the E- field:

$$\nabla \times (\frac{1}{\mu_r} \nabla \times \mathbf{E}) - k^2 \epsilon_r \mathbf{E} = 0 \tag{3.6}$$

Equation (3.6) makes it clear that the curl-curl operator reduces any vector function expressed as the gradient of a scalar function to zero, which results in a zero eigenvalue solution. The Nedelec constraints reduce the number of zero eigenvalues, which correspond to spurious solutions. Inspection of this vector function (3.5) reveals that the x component is linear in y and the y component is linear in x. This is sometimes referred to as a half order function, since it is linear in x (or y) and constant in x (or y). This is the form of the vector approximation which is proposed and more descriptively referred to as a CT/LN basis function. The CT/LN property results from the combination of basis functions of the form (3.5), and in this 2D case three basis functions will be employed to obtain the three degrees of freedom. These are the first three functions listed in table 3.1. In the same manner, a complete quadratic function with 8 degrees of freedom is reduced to 6 degrees of freedom, using constraints determined by Nedelec [11]. Now all of the six basis functions in table 3.1 are included and the approximation is referred to as LT/QN. These were all calculated and plotted in figures 3.2 to 3.9 over a typical element. Jin [2, p. 236] also shows plots of the first three basis functions.

3.2.1 CT/LN Approximation

These basis functions produce constant tangential components and linear normal components on element boundaries. The form of the basis functions as suggested by Webb [4] was chosen and is given in table 3.1. The three basis functions are shown on a typical element in figures 3.2, 3.3 and 3.4. These are vector functions and are associated with the edge on which it has both a tangential and a normal component. The function has normal components on all three edges, but only on one edge does it have a tangential component. This can be seen on the above figures. A distinction must be made between the properties of a single basis function and that of the combined effect. It is instructive to examine a single function with the form of the first three functions given in table 3.1.

Stellenbosch University https://scholar.sun.ac.za

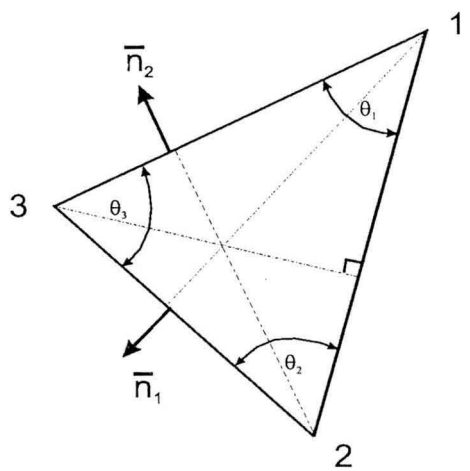

Figure 3.1: The geometry of the simplex element.

Edge Contributions of a Single CT/LN Basis Function

In the 2D case a useful identity is found in [10] which will be used to decompose the basis function into normal and tangential components with respect to the element boundaries:

$$\nabla\lambda_i = -\frac{\hat{\mathbf{n}}_i}{h_i} \tag{3.7}$$

h_i is the height of the triangle from base i, while $\mathbf{n}_i$ is the unit normal to this edge. Refer to figure 3.10 for the numbering of triangle edges and appendix A. One of the vector functions will be $-\lambda_i(\frac{\hat{\mathbf{n}}_j}{h_j}) + \lambda_j(\frac{\hat{\mathbf{n}}_i}{h_i})$, where use was made of (3.7). Consider the contribution on each of the edges:
edge (i,k) : $\lambda_j = 0$, leaving only a normal component $-\frac{\lambda_i}{h_j}$
edge (k,j) : $\lambda_i = 0$, leaving only a normal component $\frac{\lambda_j}{h_i}$
edge (i,j) : a tangential and normal component is found on this edge. Now the combination of these functions to obtain the degrees of freedom described by Nedelec [11] is described. Consider the E- field expressed in terms of the basis functions:

$$\begin{aligned}\mathbf{E} &= E_1\mathbf{w}_{12}^{(0.5)} + E_2\mathbf{w}_{23}^{(0.5)} + E_3\mathbf{w}_{31}^{(0.5)} \\ &= \nabla\lambda_1(-E_1\lambda_2 + E_3\lambda_3) + \nabla\lambda_2(E_1\lambda_1 - E_2\lambda_3) + \nabla\lambda_3(E_2\lambda_2 - E_3\lambda_1)\end{aligned} \tag{3.8}$$

Here E_i is defined as $\ell_i \cdot e_i$, which incorporates the length of the element edge with the constant E_i. (3.8) is rewritten in terms of normal components with the use of (3.7)

$$\mathbf{E} = -\frac{\hat{\mathbf{n}}_1}{h_1}(-E_1\lambda_2 + E_3\lambda_3) - \frac{\hat{\mathbf{n}}_2}{h_2}(E_1\lambda_1 - E_2\lambda_3) - \frac{\hat{\mathbf{n}}_3}{h_3}(E_2\lambda_2 - E_3\lambda_1) \tag{3.9}$$

Consider now the contribution on an edge, for example edge (2,3) and note that

$$\begin{aligned}\lambda_1 &= 0 \\ \lambda_2 + \lambda_3 &= 1 \\ \nabla\lambda_2 &= -\nabla\lambda_3\end{aligned} \tag{3.10}$$

Stellenbosch University https://scholar.sun.ac.za

On edge(2,3), the field in (3.9) is reduced to

$$\mathbf{E}_{23} = -\frac{\hat{n}_1}{h_1}[-\lambda_2(E_1 + E_3) + E_3] + E_2\frac{\hat{n}_2}{h_2} \tag{3.11}$$

with the use of (3.10).

Tangential component on edge (2,3)

Let $\hat{t}_{23}$ be the tangential unit vector to edge (2,3). From figure 3.1, it can be derived that $\hat{t}_{23} \cdot \hat{n}_2 = -\sin(\theta_3)$. The tangential component is $-\frac{\sin\theta}{h_2}$, which can be reduced to simply $-e_2$. This shows that the tangential edge contribution is a constant. It is true in general for every one of the three edges.

Normal component on edge (2,3)

From figure 3.1, it can be shown that $\hat{n}_1 \cdot \hat{n}_2 = -\cos\theta_3$. The normal component magnitude is now $-\left(\frac{E_3}{h_1} + \frac{\cos\theta_3 E_2}{h_2}\right) + \lambda_2\frac{E1+E3}{h_1}$. Finally the approximated field on edge (2,3) is

$$-e_2\hat{t}_{23} - \{\frac{E_3}{h_1} + \frac{\cos\theta_3 E_2}{h_2} + \lambda_2\frac{E1+E3}{h_1}\}\hat{n}_{23} \tag{3.12}$$

It is clear from (3.12) that the tangential component is constant and the normal component is linear in a simplex coordinate. Hence these basis functions combine to form the CT/LN basis set.

3.2.2 LT/LN Basis functions

These basis functions produce linear tangential and linear normal components on element edges. The first six functions of table 3.1 forms Webb's LT/LN basis set. The approximation was implemented and found that this higher order approximation is less accurate than the lower order CT/LN approximation. This is a surprising result, and an explanation was required. On investigation it was found that the form suggested by Webb [4] contained a linear dependence and should not be used. However, a slightly altered form works well, although it is not optimal. Dibben and Metataxis [16], who referred to their LT/LN element as a "linear element", remarked on this fact and showed that although the rate of convergence is higher as the mesh is refined, the average error is higher for the linear element (LT/LN in the terminology used here) than for the standard CT/LN approximation.

3.2.3 LT/QN Basis functions

These basis functions produce linear tangential and quadratic normal components on element boundaries. When a more accurate approximation of the field variable is required, one could increase the number of basis functions to 8 as shown in table 3.1, to obtain a LT/QN approximation. The last two basis functions are face functions. These are associated with the face of a triangle (or the face of a tetrahedron in 3D) since there is no tangential contribution on any edge of the element. This property can be seen from figures 3.8 and 3.9. Also there is no contribution, tangential or normal, on two edges. In this way tangential continuity between elements, which was established previously by enforcing tangential continuity for the first 6 basis functions, is not affected. These face functions add normal components to two of the three edges, which introduce the quadratic normal components.

Stellenbosch University https://scholar.sun.ac.za

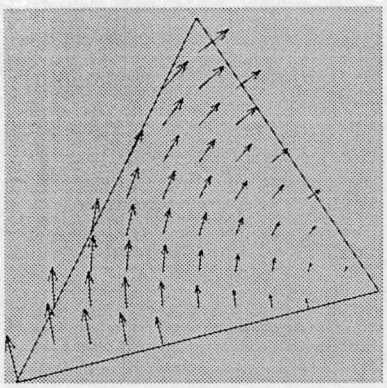

Figure 3.2: The first basis function over an element.

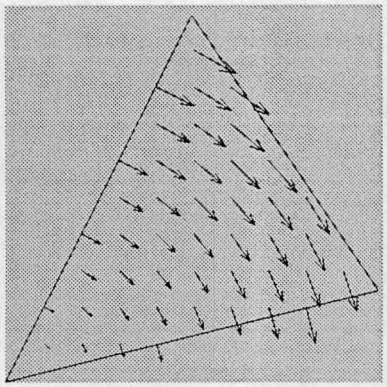

Figure 3.3: The second basis function over an element.

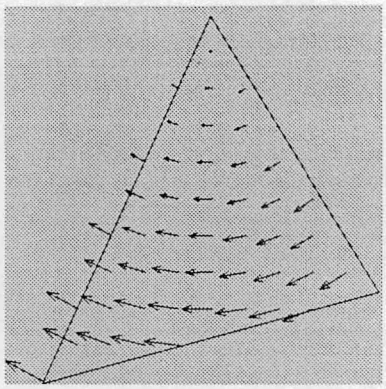

Figure 3.4: The third basis function over an element.

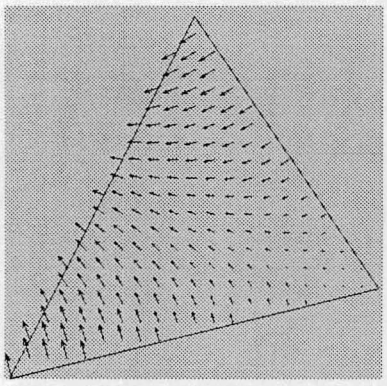

Figure 3.5: The fourth basis function over an element.

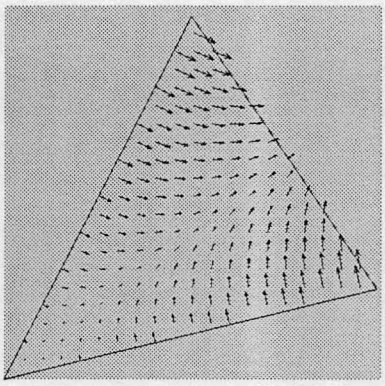

Figure 3.6: The fifth basis function over an element.

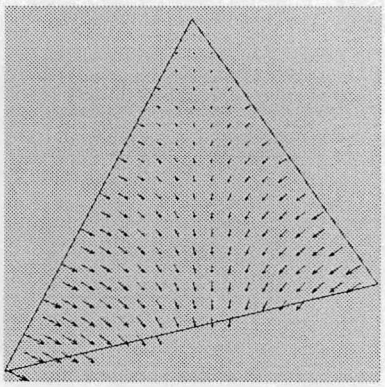

Figure 3.7: The sixth basis function over an element.

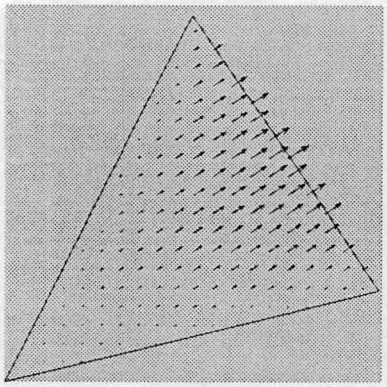

Figure 3.8: The seventh basis function (face function) over an element.

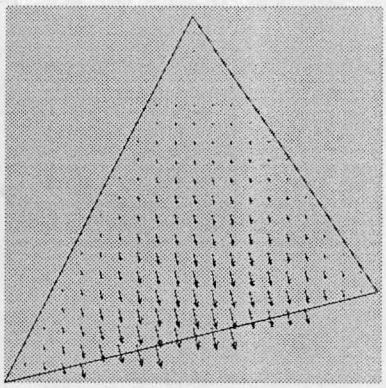

Figure 3.9: The eighth basis function (face function) over an element.

Stellenbosch University https://scholar.sun.ac.za

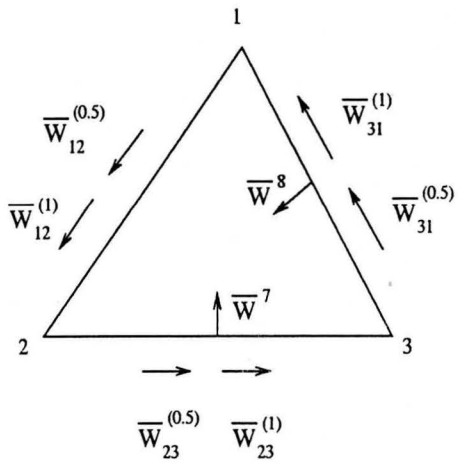

Figure 3.10: Edge-based functions and the degrees of freedom for a triangular element. Reprinted from [17].

The E field expressed in terms of the 8 basis functions and the 8 coefficients is

$$\begin{aligned}\mathbf{E} &= E_1\mathbf{w}_{12}^{(0.5)} + E_2\mathbf{w}_{23}^{(0.5)} + E_3\mathbf{w}_{31}^{(0.5)} + E_4\mathbf{w}_{12}^{(1)} + E_5\mathbf{w}_{23}^{(1)} + E_6\mathbf{w}_{31}^{(1)} + e_7\mathbf{f}_1 + e_8\mathbf{f}_2 \\ &= \nabla\lambda_1\left[\lambda_2(E_4 - E_1) + \lambda_3(E_3 + E_6) + e_7\lambda_2\lambda_3\right] \\ &+ \nabla\lambda_2\left[\lambda_1(E_1 + E_4) + \lambda_3(E_5 - E_2) + e_8\lambda_1\lambda_3\right] \\ &+ \nabla\lambda_1(E_6 - E_3) + \lambda_2(E_2 + E_5)) \end{aligned} \tag{3.13}$$

(the face coefficients are indicated with e_i since the E_i includes the edge length)

Here it is clear that quadratic terms in the simplex elements are introduced. This is also quadratic in Cartesian coordinates, since the simplex coordinates are linear in x and y. The face functions introduces an unsymmetric approximation over each element.

These were the highest order of approximation implemented, however it is possible to introduce more basis functions associated with higher order approximations. However, the computational cost increases rapidly with higher orders and it would be even more apparent in three dimensional modelling.

3.3 Derivation of the S matrix : LT/QN

The element matrix for the CT/LN case in two dimensions is derived by Jin [2]. However, the LT/QN element matrices have not appeared before and had to be derived.

The E-field is expressed in terms of the eight vector basis functions

$$\mathbf{E} = \sum_{m=1}^{3} E_m\mathbf{w}_m^{(0.5)} + \sum_{m=4}^{6} E_m\mathbf{w}_m^{(1)} + \sum_{m=7}^{8} e_m\mathbf{w}_m^{(1.5)} \tag{3.14}$$

These basis functions are defined in table 3.1.

To derive the S-matrix, $\nabla \times \overline{E}$ must be calculated.

Stellenbosch University https://scholar.sun.ac.za

$$[S]_{mn} = \int_{\Omega} \frac{1}{\nabla} \times \mathbf{w}_m \cdot \nabla \times \mathbf{w}_n d\Omega \tag{3.15}$$

This was done by Lee and Mittra [3] for the first three basis functions in the 3D case. Here the notation of Jin [2] will be followed.

Using vector identities it can be shown that $\nabla \times \overline{w}_{ij}^{(1)} = 0$. This results in an 8 by 8 S-matrix, containing the submatrix $S_{CT/LN}$ for the half order basis function described in [2], some of the rest filled with zeros and the submatrix S_{face}, which results from the added face functions.

$$\begin{bmatrix} [S_{CT/LN}] & [0] & [0] \\ [0] & [0] & [0] \\ [0] & [0] & [S_{face}] \end{bmatrix} \tag{3.16}$$

The S matrix for the LT/QN case is now

$$S = \frac{1}{A} \begin{bmatrix} \ell_1^2 & & & & & & & \\ \ell_1\ell_2 & \ell_2^2 & & & & & & \\ \ell_1\ell_3 & \ell_2\ell_3 & \ell_3^2 & & & & & \\ 0 & 0 & 0 & 0 & & & & \\ 0 & 0 & 0 & 0 & 0 & & & \\ 0 & 0 & 0 & 0 & 0 & 0 & & \\ 0 & 0 & 0 & 0 & 0 & 0 & 1/8 & \\ 0 & 0 & 0 & 0 & 0 & 0 & 5/48 & 1/8 \end{bmatrix} \tag{3.17}$$

where A is the area of the element.

3.4 Derivation of the T matrix : LT/QN

The T matrix is symmetric as seen from (3.18):

$$[T]_{mn} = \int_{\Omega} \overline{\tau}_m \cdot \overline{\tau}_n d\Omega \tag{3.18}$$

Only the lower part of the symmetric T matrix is shown here, as calculated for the 2D LT/QN approximation.

Stellenbosch University https://scholar.sun.ac.za

$$T = \frac{1}{48A}\begin{bmatrix}
2(f_{22}+f_{11}) & -f_{12} & & & & & & & & & & \\
(f_{12}-f_{13}) & +f_{23}-f_{22}) & 2(f_{33}+f_{22}) & -f_{23}) & & & & & & & & \\
(f_{12}-f_{11}) & +f_{13}-2f_{23}) & (f_{31}-2f_{12}) & +f_{23}-f_{33}) & 2(f_{11}+f_{33}) & -f_{13}) & & & & & & \\
2(f_{22}) & -f_{11}) & (f_{23}-f_{22}) & -f_{12}+2f_{13}) & (f_{12}+f_{11}) & -f_{13}-2f_{23}) & 2(f_{22}f_{12}) & +f_{11}) & & & & \\
(f_{23}-2f_{13}) & -f_{12}+f_{22}) & 2(f_{23}) & -f_{22}) & (f_{13}+f_{33}) & -f_{23}+2f_{12}) & (2f_{13}+f_{12}) & +f_{22}+f_{23}) & 2(f_{33}+f_{22}) & +f_{23}) & & \\
(f_{21}-f_{11}) & -f_{13}+2f_{23}) & (f_{31}-2f_{12}) & +f_{23}+f_{33}) & 2(f_{11}) & -f_{33}) & (f_{12}+f_{11}) & +f_{13}+2f_{23}) & (f_{13}+f_{33}) & +f_{23}+2f_{12}) & 2(f_{11}+f_{33}) & +f_{13}) \\
(f_{12}) & -2f_{11}) & (2f_{13}) & -2f_{12}) & (2f_{11}) & -f_{13}) & (f_{12}) & +2f_{11}) & 2(f_{13}) & +f_{12}) & (2f_{11}) & +f_{13}) & 2/3f_{11} & \\
(2f_{22}) & -f_{12}) & (f_{23}) & -2f_{22}) & 2(f_{22}) & -f_{12}) & (2f_{22}) & +f_{12}) & (f_{23}) & +2f_{22}) & 2(f_{22}) & +f_{12}) & 1/2f_{12} & 2/3f_{22}
\end{bmatrix} \tag{3.19}$$

f_{ij} is defined

$$f_{ij} = b_i b_j + c_i c_j \tag{3.20}$$

with b_i and c_i the same constants defined with simplex coordinates. Refer to Appendix A for a definition of these constants.

The CT/LN S and T matrices are found by taking the top left 6x6 submatrix from the above matrices. This is possible since hierarchical basis function were implemented.

3.5 Application to Guided Wave Problems

The matrix equation (1.7) is an eigenvalue problem, which means that there are a number of solutions for k, the cutoff frequencies of each mode, and corresponding to every k there is a solution for **U**.

The code was applied to the calculation of the cutoff frequencies of propagating modes in cylinders of possible arbitrary cross section, for both the TE and TM modes.

The mesh generation was done by the use of Delaunay triangulation code which is available in Matlab version 5. A short description of the Delaunay triangulation technique is given in appendix D. Advantage may be taken of symmetry, which reduces the number of unknowns to be solved. One must be careful to ensure that non-symmetric modes are not lost if this is done.

Stellenbosch University https://scholar.sun.ac.za

Recall from section 1.2 that $\mathbf{U}$ is either the E-field $\mathbf{E}$ or H field $\mathbf{H}$. The energy functional is

$$F(\mathbf{U}) = \frac{1}{2}\iint_S (\frac{1}{p_r}(\nabla \times \mathbf{U}) \cdot (\nabla \times \mathbf{U}) - k_0^2 q_r \mathbf{U} \cdot \mathbf{U}) dS \tag{3.21}$$

The boundary conditions at a perfectly conducting surface are

$$\begin{aligned} \hat{n} \times \mathbf{E} &= 0 \\ \hat{n} \cdot \mathbf{B} &= 0 \end{aligned} \tag{3.22}$$

where $\hat{n}$ is defined in the usual manner. Now either the TE or TM modes can be found by substituting the correct field variable and the relative material parameters in the correct positions.

3.5.1 TE Modes

In this case $\mathbf{U} = \mathbf{E}$ and $p = \mu_r, q = \epsilon_r$. The TE modes have no z directed E- field, so that the E-field is contained in the transverse plane. This enables the discretisation of the 2D transverse plane cross-section of the waveguide. The boundary condition enforced is the essential boundary condition which constrains the tangential E- field on the boundary to zero. This must be enforced explicitly.

3.5.2 TM Modes

Let $\mathbf{U} = \mathbf{H}$ and $p = \epsilon_r, q = \mu_r$. Now there is no z-directed H- field. Once again the transverse plane cross-section is discretised. The boundary condition is the natural boundary condition $\hat{n} \cdot \mathbf{D} = 0$ or $\hat{n} \cdot (\nabla \times \mathbf{H}) = 0$ which is equivalent since $\mathbf{E}$ is time-varying [1, p. 98-99]. It is implemented by leaving the edge H- fields unconstrained, the boundary condition is implied and comes naturally with the energy functional (3.21). A requirement or boundary condition that is not mentioned since it is rather obvious, is that the field variable must be continuous along adjacent edges. This is enforced by the FEM element connection procedure.

3.6 Conclusion

In this chapter, the hierachical basis functions were listed and the properties as a result of the form discussed. It is shown that the normal components on element edges are approximated with one order higher than the tangential components on element edges. S and T matrices were derived. The next step is to apply the theory to realistic problems of engineering importance.

Stellenbosch University https://scholar.sun.ac.za

Chapter 4

Results for Circular and Ridged Waveguides

4.1 Introduction

In this chapter results are presented for 2D eigenvalue problems. The first aim is to examine the reliability and accuracy of the formulation by application to a simple problem: that of a circular cross-section waveguide, so that a comparison with analytic data can be made. Ridged waveguides will then be examined and field plots generated.

4.2 Circular Waveguides

The code was applied to calculate the cutoff frequencies of propagating modes in circular cylinders of infinite length and radius 1 m, for the TE and TM modes. The accuracy of CT/LN and LT/QN approximations is examined by comparing the values calculated with the FEM technique to the exact cutoff frequencies. In both cases the entire cross-section of the waveguide was discretised into 200 elements. For the CT/LN approximation there were 280 degrees of freedom and for the LT/QN approximation there were 960 degrees of freedom.

From tables 4.1 and ?? it can be seen that the LT/QN solutions are in most cases (but not always) more accurate than the CT/LN solutions. This result agrees with Savage and Peterson's comment in [5, p.878] : "Although the convergence of any particular eigenvalue is usually erratic, the general error behaviour of the two methods is apparent when the average error of several modes is visualised". The two methods referred to here are a low order and high order approximation, respectively. Also note that for the TM case the average error is higher. This can be explained by the fact that normal continuity conditions are implied by the formulation, but are dependent on an integration over the entire structure.

Stellenbosch University https://scholar.sun.ac.za

Peterson [9] published his results for the circular cylinder with radius one wavelength and infinite length. He found that some wave numbers appeared more than once and remarked that these repeated values "appear to represent genuine wavenumbers". When the corresponding field plots are drawn it becomes clear what these values represent. Figures 4.3 and 4.4 correspond to wavenumbers 1.8454 (the TE_{11} mode) and 1.8382 which is a mode with a similar field distribution but different orientation with respect to the central axis. This latter mode is a degenerate mode. From table 4.1 it is evident that there are a number of these modes. Figures 4.6 and 4.8 also illustrate this, figure 4.6 is the genuine TE_{21} mode, while figure 4.8 is a degenerate mode. Degenerate modes have identical cutoff frequencies but different field distributions [18]. These may exist physically in contrast to spurious modes which are entirely non-physical and cannot exist.

4.3 Ridged Waveguides

Ridged waveguides are known to lower the cutoff frequency of the TE_{10} mode while increasing the cutoff frequencies of the higher order modes, resulting in a larger bandwidth. Possible configurations are single, double and quadruple ridged waveguides. [19, p. 457].

4.3.1 Double Ridged Waveguide

The waveguide parameters as defined in figure 4.1 were $b/a = 0.45$, $d/b = 0.5$ and $s/a = 0.4$. The cross-section was discretised into a uniform mesh of 128 triangular elements.

No analytical solution is available for this type of waveguide, but approximations are available for the cutoff wavelength of the first mode [20]. These results have a maximum error of between 1 and 3 percent according to Pyle [20] for the worst case where $s/a << 1$. The results are compared in table 4.3.

E- field vector plots for the first four TE modes are shown in figures 4.15 to 4.18. The change of direction of the E- field at the corners is made possible by the vector basis functions.

4.3.2 Single Ridged Waveguide

The waveguide parameters as defined in figure 4.2 were $b/a = 0.45$, $d/b = 0.5$ and $s/a = 0.4$. The cross-section was discretised into a uniform mesh of 128 triangular elements.

Once again an approximation for the TE_{10} mode is given in [20]. The results are compared in table 4.4. E- field vector plots for the first four TE modes are shown in figures 4.19 to 4.22.

4.4 Circular Waveguide Loaded with Eccentric Dielectric Cylinder

In the previous applications, the guiding structures were air-filled. One of the strengths of the FEM technique is the ease with which inhomogeneously filled guides can be analysed. This application was chosen to demonstrate this.

Stellenbosch University https://scholar.sun.ac.za

Exact TE wavenumbers (first 6)	CT/LN	LT/QN	CT/LN error %	LT/QN error %
1.841	1.8482	1.8382	0.391	-0.152
	1.8482	1.8454	0.391	0.239
3.054	3.0674	3.0430	0.439	-0.344
	3.0797	3.0461	0.842	-0.259
3.831	3.8274	3.8030	-0.094	-0.731
4.19	4.2273	4.1654	0.890	-0.587
	4.2273	4.1675	0.890	-0.537
5.317	5.3223	5.2128	0.156	-1.546
	5.3323	5.2298	0.156	-1.64
		5.2462		-1.332
5.331	5.3325	5.2944	0.028	0.0687
	5.3525	5.3518	0.3	0.39

Table 4.1: The TE modes: exact and calculated for circular waveguide radius 1 m. The guide cross-section was discretised into 200 elements.

Exact TM wavenumbers (first 6)	CT/LN	LT/QN	CT/LN error %	LT/QN error %
2.405	2.4201	2.4016	0.628	-0.141
3.832	3.8547	3.7971	0.592	-0.911
	3.8547	3.8296	0.592	-0.00626
5.136	5.1731	5.0729	0.722	-0.8392
	5.1953	5.0814	1.154	-1.0631
5.520	5.5204	5.4499	0.0072	-1.2771
6.380	6.4543	6.2432	1.1646	-2.1442
	6.4453	6.2632	1.0235	-1.831
7.016	7.009	6.7520	-0.09977	-3.7628
	7.009	6.9518	-0.09977	-0.915
7.558	7.6738	7.3315	1.5321	-2.997
	7.7043	7.3602	1.936	-2.617

Table 4.2: The TM modes: exact and calculated for circular waveguide radius 1 m. The guide cross-section was discretised into 200 elements.

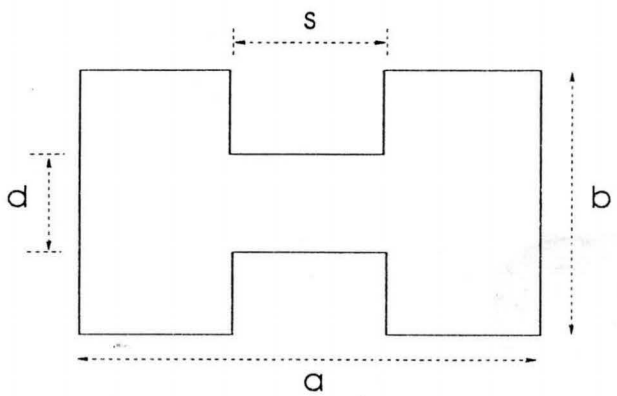

Figure 4.1: Dimensions of the cross-section of a double ridged waveguide.

Stellenbosch University https://scholar.sun.ac.za

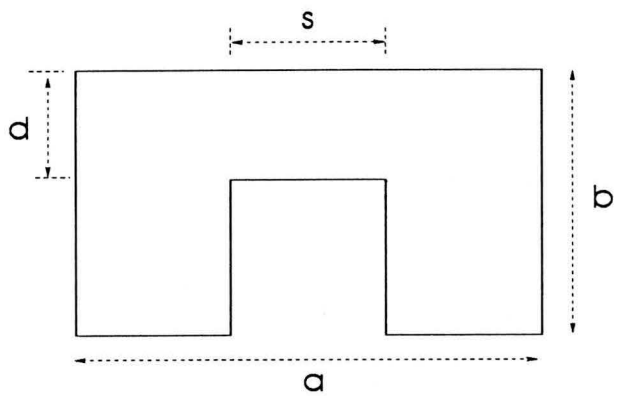

Figure 4.2: Dimensions of the cross-section of a single ridged waveguide.

Pyle's TE cutoff wavelength $(\frac{\lambda_c}{a})$	CT/LN result $(\frac{\lambda_c}{a})$	LT/QN result $(\frac{\lambda_c}{a})$
2.652	2.7338	2.664
-	1.0718	1.0200
-	0.8816	0.8772
-	0.8807	0.8764
-	0.6625	0.6448

Table 4.3: The TE modes: Pyle's approximation for TE_{10} cutoff wavelength (normalised by a) and FEM results for a double ridged waveguide. The guide cross-section was discretised into 64 elements.

Pyle's TE cutoff wavelength $(\frac{\lambda_c}{a})$	CT/LN result $(\frac{\lambda_c}{a})$	LT/QN result $(\frac{\lambda_c}{a})$
2.785	2.8318	2.7914
-	1.1983	1.1666
-	0.8806	0.8742
-	0.7991	0.8001
-	0.656	0.6433

Table 4.4: The TE modes: Pyle's approximation for TE_{10} cutoff wavelength (normalised by a) and FEM results for a single ridged waveguide. The guide cross-section was discretised into 128 elements.

Stellenbosch University https://scholar.sun.ac.za

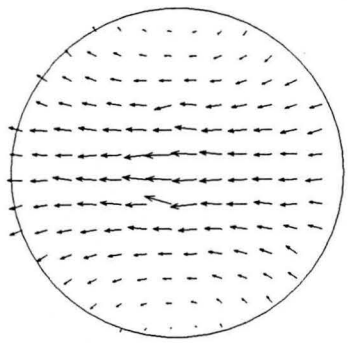

Figure 4.3: Calculated E- field configuration for k=1.8382 mode; LT/QN approximation, 200 element discretisation.

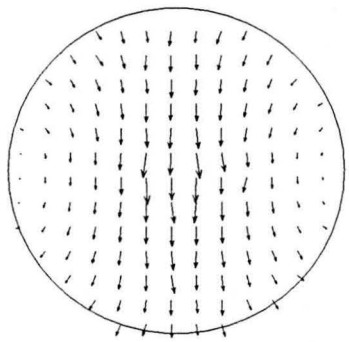

Figure 4.4: Calculated E- field configuration for k=1.8454 mode; LT/QN approximation, 200 element discretisation.

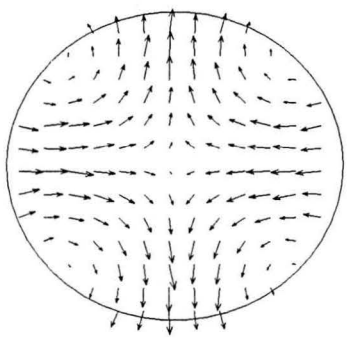

Figure 4.5: Calculated E- field configuration for k=3.0430 mode; LT/QN approximation, 200 element discretisation.

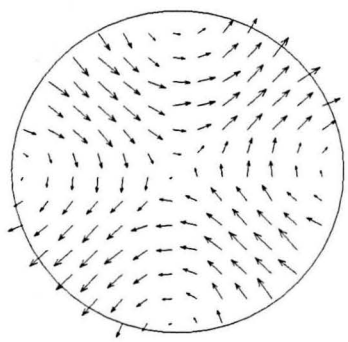

Figure 4.6: Calculated E- field configuration for k=3.0461 mode; LT/QN approximation, 200 element discretisation.

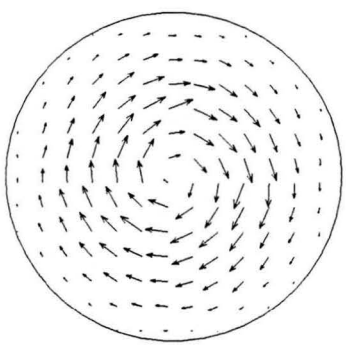

Figure 4.7: Calculated E- field configuration for k=3.8030 mode; LT/QN approximation, 200 element discretisation.

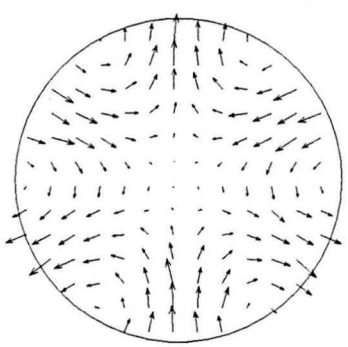

Figure 4.8: Calculated E- field configuration for k=4.1654 mode; LT/QN approximation, 200 element discretisation.

Stellenbosch University https://scholar.sun.ac.za

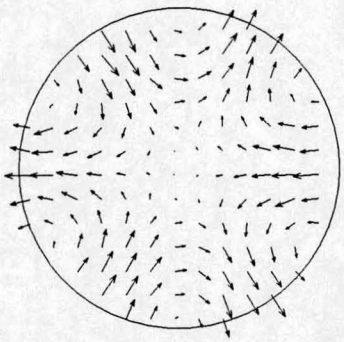

Figure 4.9: Calculated E- field configuration for k=4.1675 mode; LT/QN approximation, 200 element discretisation.

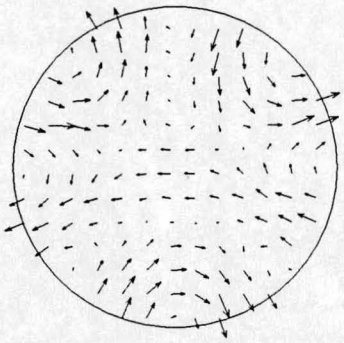

Figure 4.10: Calculated E- field configuration for k=5.2298 mode; LT/QN approximation, 200 element discretisation.

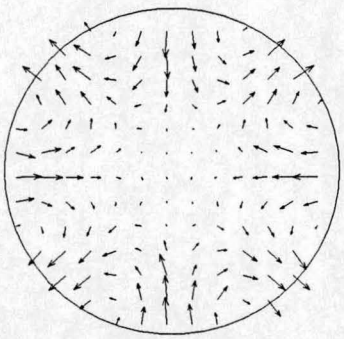

Figure 4.11: Calculated E- field configuration for k=5.2462 mode; LT/QN approximation, 200 element discretisation.

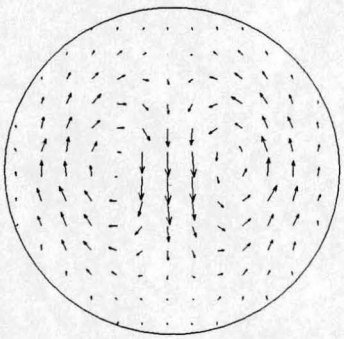

Figure 4.12: Calculated E- field configuration for k=5.2944 mode; LT/QN approximation, 200 element discretisation.

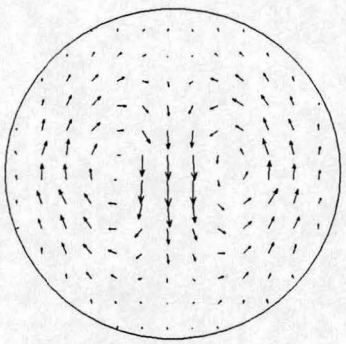

Figure 4.13: Calculated E- field configuration for k=5.2944 mode; LT/QN approximation, 200 element discretisation.

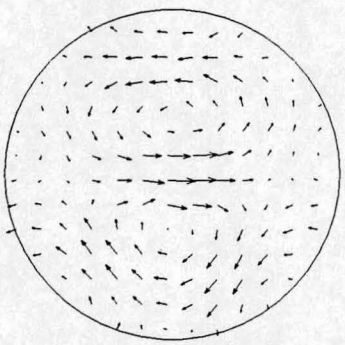

Figure 4.14: Calculated E- field configuration for k=5.3525 mode; LT/QN approximation, 200 element discretisation.

Stellenbosch University https://scholar.sun.ac.za

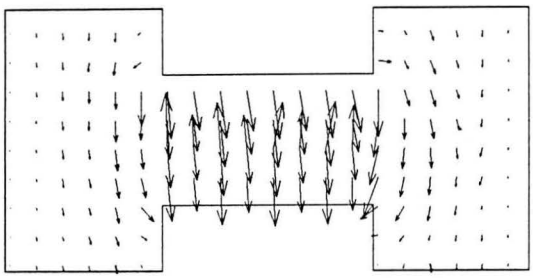

Figure 4.15: Calculated E field configuration for TE_{10} mode; LT/QN approximation, 128 element discretisation.

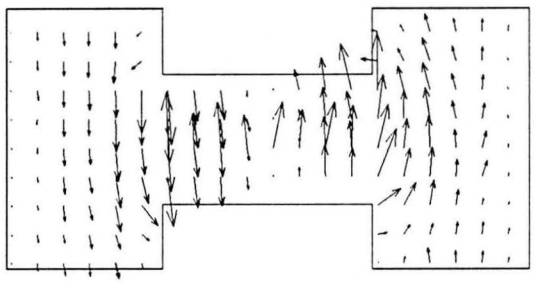

Figure 4.16: Calculated E field configuration for second mode; LT/QN approximation, 128 element discretisation.

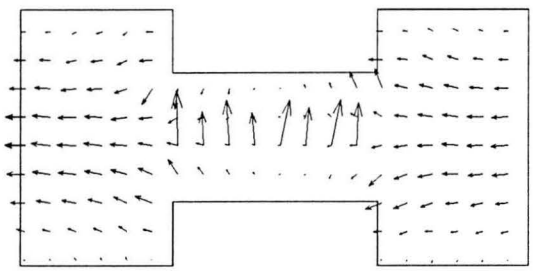

Figure 4.17: Calculated E field configuration for third mode; LT/QN approximation, 128 element discretisation.

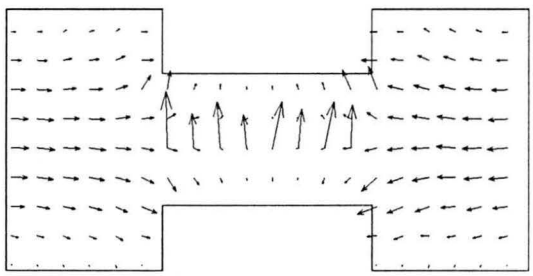

Figure 4.18: Calculated E field configuration for fourth mode; LT/QN approximation, 128 element discretisation.

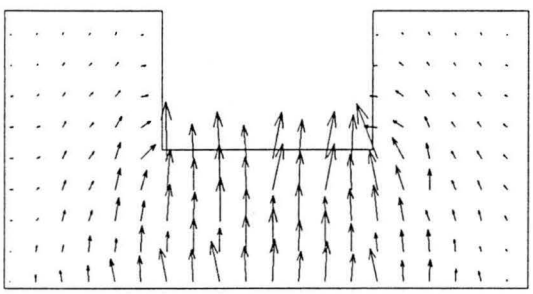

Figure 4.19: Calculated E field configuration for TE_{10} mode; LT/QN approximation, 128 element discretisation.

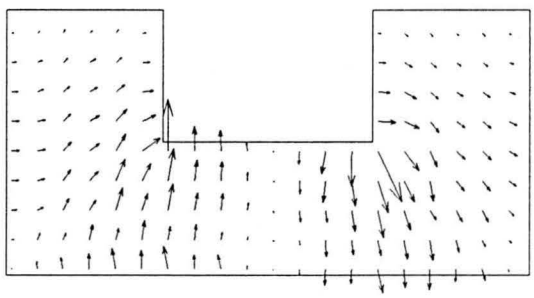

Figure 4.20: Calculated E field configuration for second mode; LT/QN approximation, 128 element discretisation.

Stellenbosch University https://scholar.sun.ac.za

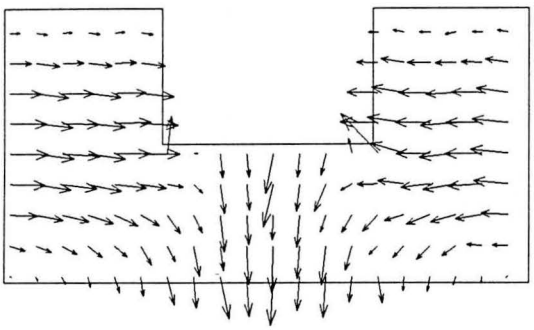

Figure 4.21: Calculated E field configuration for third mode; LT/QN approximation, 128 element discretisation.

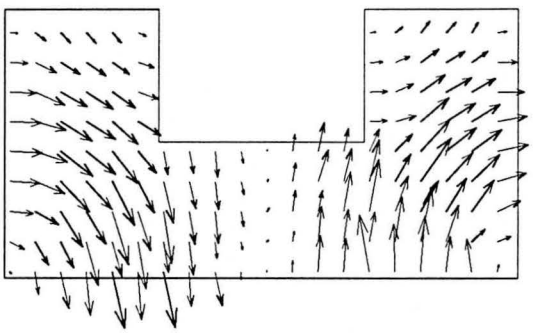

Figure 4.22: Calculated E field configuration for fourth mode; LT/QN approximation, 128 element discretisation.

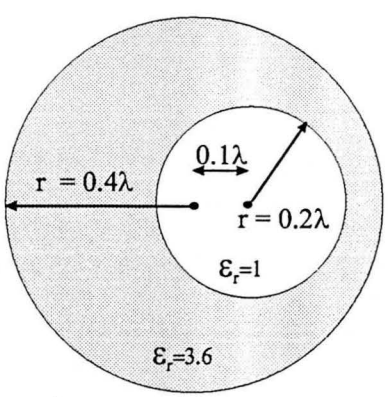

Figure 4.23: Dimensions of the cross-section of the eccentrically loaded dielectric cylinder.

Stellenbosch University https://scholar.sun.ac.za

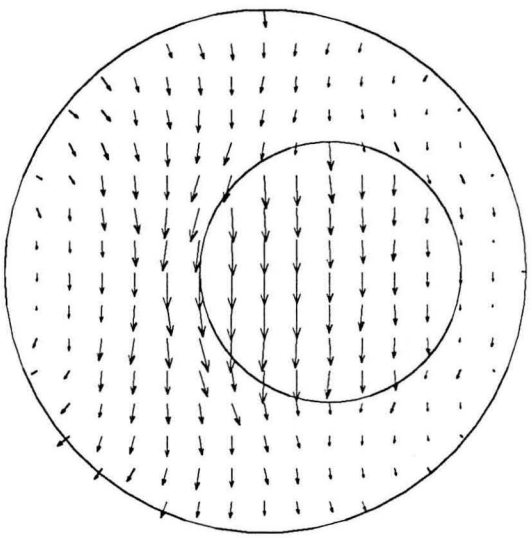

Figure 4.24: Calculated E field configuration for k=2.97 mode; CT/LN approximation, 174 element discretisation.

The cylinder has radius 0.4 wavelengths, and the inner part has $\epsilon_r = 1$, while the outer part has $\epsilon_r = 3.6$. The inner radius is 0.2 wavelengths and the distance between the centres of the cylinders is 0.1 wavelengths.

Figures 4.24, 4.25 and 4.26 show the E -field distribution for various wavenumbers. The patterns can not be confirmed with published results, but the E-field lines "bend away" from the area with lower dielectric constant, as expected and the results seem to be correct. The boundaries of the structure have been superimposed on the field plot to assist with interpretation of the results.

4.5 Conclusion

The wavenumbers calculated compare quite well with the known values in the circular waveguide case, while the results for the ridged waveguides also compare well with the approximate wavenumbers calculated by Pyle. Field plots of the E-field distribution were included to present the results in a graphical way, also confirming their validity. In the case of the circular waveguide, these plots may be compared with ones in [19, p.480-481]. The field distribution inside the ridged waveguide for various modes and the loaded circular waveguide were calculated. These were also as expected. Thus it is found that the edge- based Finite Element method for eigenvalue configurations provides reliable results.

Stellenbosch University https://scholar.sun.ac.za

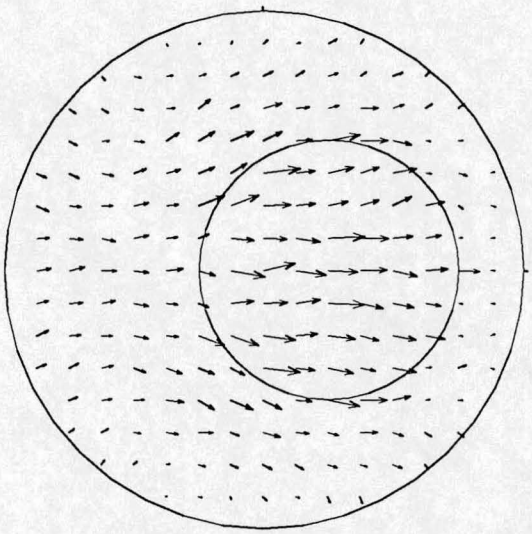

Figure 4.25: Calculated E field configuration for k=3.05 mode; CT/LN approximation, 174 element discretisation.

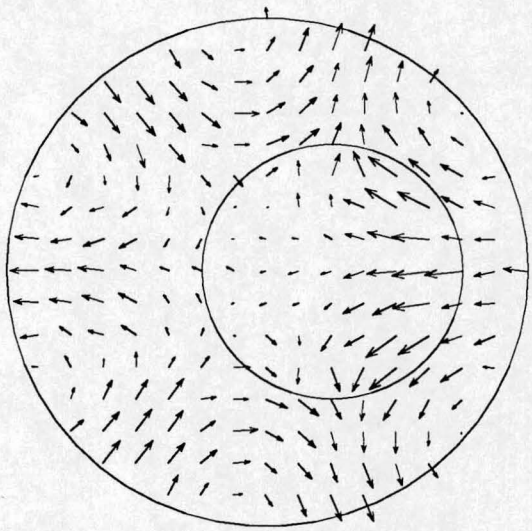

Figure 4.26: Calculated E field configuration for k=6.06 mode; CT/LN approximation, 174 element discretisation.

Stellenbosch University https://scholar.sun.ac.za

Chapter 5

Two- dimensional Scattering Problems

5.1 Introduction

Often the problem domain is infinite, which requires some form of termination. Scattering configurations are examples of these. Absorbing boundary conditions may be implemented, or possibly artificial absorbers. Here the approach followed was to divide the problem domain into two regions. The Finite Element Method is applied in the interior region, and a Boundary Element Method or Boundary Integral Method on the boundary between the regions. The two regions are coupled by fictitious surface currents. This is a hybrid technique referred to as the FEM-BEM (Finite Element- Boundary Element method). The formulation and application pertaining to two- dimensional configurations will be discussed.

Scattering from arbitrary three dimensional bodies solved by the FEM-BEM method is discussed by both [1] and [2]. In the first reference a weighted residual formulation (Galerkin) is used, while Jin chose to use a variational formulation. However, these are essentially equivalent. Jin's formulation is adapted here for the 2D case, which is not described explicitly or to be found in the literature.

An excellent overview article by Jin [21] discusses the principles of coupled FE-BI (Finite Element- Boundary Integral) methods and serves as an useful introduction.

5.2 FEM-BEM Formulation

5.2.1 Geometry

The scatterer is surrounded by a fictitious contour, C, which encloses the scatterer as tightly as possible to minimise computational effort. All non-homogeneous material must be enclosed by C. In this way the infinite problem domain is divided into two regions which are separated by C. The infinite surface must be closed, therefore it is surrounded by another contour, C_{inf}, which is infinitely far away from the scatterer.

Stellenbosch University https://scholar.sun.ac.za

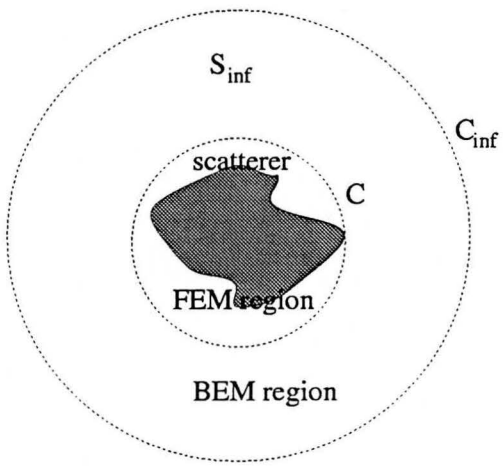

Figure 5.1: FEM-BEM geometry. Here C_∞ represents a contour enclosing S_∞ at a distance infinitely far away from the scatterer.

A much simpler problem to solve would have been that of sources specified in an infinite free space region, since the free space Green's functions are known and the field variable may be calculated over the whole domain. The problem will now be reduced to this simpler configuration. Effective surface currents are formulated on C, which represent the effect of the non-homogenous material. Note that the surface currents are still unknown at this stage. Now there are two decoupled regions :

Region 1 (BEM region) The infinite free space area outside C, with surface currents on a contour C as sources.

Region 2 The area inside C with surface currents specified on C, ensuring continuity between region 1 and 2. To solve for the scattered fields, it is necessary to solve for the field variable(E or H) over the whole of the area enclosed by C, as well as for the fictitious surface currents on C.

5.2.2 Key steps

- An integral equation relating the field variable over the problem domain with the relevant Green's function is developed.
- The integration in the integral equation above involves an integration over an infinite domain. This is now rewritten as integration over the bounding contour of the surface.
- After some manipulation the E- field (or H- field) is expressed as the sum of the incident field and a term involving the surface current sources and the relevant Green's function. It can be represented as

Stellenbosch University https://scholar.sun.ac.za

$$\mathbf{E} = \mathbf{E_{inc}} + L_M(\hat{\mathbf{m}}' \times \nabla' \times \mathbf{E}(\mathbf{r}')) + L_J(\hat{\mathbf{m}}' \times \mathbf{E}(\mathbf{r}')) \tag{5.1}$$

where L_M and L_J are integro-differential operators.

- The equation is now written entirely in terms of the components of the field tangential to the contour C and discretised using the vector expansion as described.
- Finally the dot-product with the basis functions employed on the contour is taken and integration over the whole contour is performed. This results in one of the equations that will be used to solve for the surface currents.
- The second equation is found by applying the Finite Element technique inside C, which also includes the surface currents on C. The functional is modified to include a contribution from the boundary between the regions, which is the contour C.

5.2.3 BE treatment of the exterior region

What follows is a derivation that leads to a mathematical statement of Huygens's principle [22].

$\mathbf{E}(\mathbf{r})$ is the total field produced by the superposition of an incident field $\mathbf{E}_{inc}$ and the scattered field originating form the scatterer. $\mathbf{E}_{inc}$ is defined as the field that would be present in the absence of the scatterer.

$\mathbf{E}$ satisfies the vector Helmholtz equation:

$$\nabla \times \nabla \times \mathbf{E} - k_0^2 \mathbf{E}(\mathbf{r}) = -jk_0 z_0 \mathbf{J}(\mathbf{r}) \tag{5.2}$$

Let $\overline{\overline{G}}$ be the 2D dyadic Green's function given by

$$\overline{\overline{G}}(\overline{r}', \overline{r}) = \left[\overline{\overline{I}} + \frac{1}{k_0^2}\nabla\nabla\right] G_0(\mathbf{r}, \mathbf{r}') \tag{5.3}$$

which satisfies

$$\nabla \times \nabla \times \overline{\overline{G}}(\overline{r}', \overline{r}) - k_0^2 \overline{\overline{G}}(\overline{r}', \overline{r}) = \overline{\overline{I}}\delta(\mathbf{r} - \mathbf{r}') \quad \mathbf{r}' \in S_\infty \tag{5.4}$$

This is a function of $\mathbf{r}'$ and $\mathbf{r}$ which represent the source and observation points respectively. Note that the Green's function is symmetric with respect to these two variables, a property that will be utilised later.

Taking the dot product of (5.2) with $\overline{\overline{G}}(\overline{r}', \overline{r})$, the 2D free space dyadic Green's function, and integrating over S_∞ results in:

$$\begin{aligned} \oiint_{S_\infty} [\nabla \times \nabla \times \mathbf{E}(\mathbf{r})] \cdot \overline{\overline{G}}(\overline{r}', \overline{r}) - k_0^2 \mathbf{E}(\mathbf{r}) \cdot \overline{\overline{G}}(\overline{r}', \overline{r}) dS \\ = -\oiint_{S_\infty} jk_0 Z_0 \mathbf{J}(\mathbf{r}) \cdot \overline{\overline{G}}(\overline{r}', \overline{r}) dS \end{aligned} \tag{5.5}$$

Stellenbosch University https://scholar.sun.ac.za

The integration over an infinite (closed) surface can be replaced by integration over the contour enclosing the surface, with the use of Green's second vector- dyadic identity (Appendix C) for the 2D case

$$\oiint_{S_\infty} (\nabla\times\nabla\times\mathbf{E})\cdot\overline{\overline{G}}(\bar{r}',\bar{r}) - \mathbf{E}\cdot(\nabla\times\nabla\times\overline{\overline{G}}(\bar{r}',\bar{r}))dS$$
$$= \oint_{C_\infty}[(\hat{m}\times\mathbf{E})\cdot(\nabla\times\overline{\overline{G}}(\bar{r}',\bar{r})) + (\hat{m}\times\nabla\times\mathbf{E})\cdot\overline{\overline{G}}(\bar{r}',\bar{r})]d\ell \tag{5.6}$$

where $\hat{m} = \hat{l}\times\hat{n}$, $\hat{\ell}$ the unit vector along C and $\hat{m}$ the unit vector perpendicular to the x-y plane in which the contour C is contained. Here $\hat{n} = \hat{z}$. In this way $\hat{m}\times\vec{E}\,|_C$ is the tangential E- field on the contour C, just as $\hat{n}\times\vec{E}\,|_C$ has the same magnitude as the tangential E- field in the 3D case to a surface enclosing a volume. $\mathbf{E}$ and $\overline{\overline{G}}(\bar{r}',\bar{r})$ both satisfy the Sommerfeld radiation condition; this allows the integration over C_∞ to be reduced to an integration over the contour C. Noting that $\overline{\overline{G}}(\bar{r}',\bar{r})$ satisfies (5.4) and combining (5.2), (5.4) and (5.6) we obtain

$$\iint_{S_\infty}[\mathbf{E}(\mathbf{r})\cdot\overline{\overline{I}}\delta(\mathbf{r}-\mathbf{r}')dS + \mathbf{E}_{inc}(\mathbf{r}')$$
$$= \oint_C[\hat{m}\times\mathbf{E}(\mathbf{r})]\cdot[\nabla\times\overline{\overline{G}}(\bar{r}',\bar{r})] + [\hat{m}\times\nabla\times\mathbf{E}(\mathbf{r})]\cdot\overline{\overline{G}}(\bar{r}',\bar{r})]d\ell \tag{5.7}$$

where $\mathbf{E}_{inc}$ represents the field radiated by the source current $\mathbf{J}$. (5.7) simplifies to

$$\begin{aligned}\mathbf{E}(\mathbf{r}') &= \mathbf{E}_{inc}(\mathbf{r}')d\ell + \oint_C[(\hat{m}'\times\mathbf{E})\cdot(\nabla'\times\overline{\overline{G}}(\bar{r}',\bar{r}))\\ &+ [\hat{m}'\times\nabla\times\mathbf{E}(\mathbf{r})]\cdot\overline{\overline{G}}(\bar{r}',\bar{r})]d\ell\end{aligned} \tag{5.8}$$

$\overline{\overline{G}}(\bar{r}',\bar{r})$ is symmetric in $\mathbf{r}$ and $\mathbf{r}'$, allowing $\mathbf{r}$ and $\mathbf{r}'$ to be exchanged:

$$\begin{aligned}\mathbf{E}(\mathbf{r}) &= \mathbf{E}(\mathbf{r})_{inc}(\mathbf{r}) + \oint_C[(\hat{m}\times\mathbf{E}(\mathbf{r}')\cdot(\nabla'\times\overline{\overline{G}}(\bar{r}',\bar{r}))\\ &+ (\hat{m}\times\nabla\times\mathbf{E}(\mathbf{r}'))\cdot\overline{\overline{G}}(\bar{r}',\bar{r})]d\ell\end{aligned} \tag{5.9}$$

Using vector and dyadic identities, the expressions containing dyadics are reduced to expressions containing vectors only (see Appendix C)

$$\begin{aligned}\mathbf{E}(\mathbf{r}) &= \mathbf{E}_{inc}(\mathbf{r}) + \oint_C[\hat{m}'\times\mathbf{E}(\mathbf{r}')]\times\nabla'G_0(\mathbf{r},\mathbf{r}')) + [\hat{m}'\times\nabla'\times\mathbf{E}(\mathbf{r})]G_0(\mathbf{r},\mathbf{r}')\\ &+ \frac{1}{k_0^2}\nabla'\cdot[\hat{m}'\times\nabla'\times\mathbf{E}(\mathbf{r}')]\nabla G_0(\mathbf{r},\mathbf{r}'))d\ell\end{aligned} \tag{5.10}$$

This is valid for any $\mathbf{r}$ in S_∞, with $\mathbf{r}'$ restricted on C, where the source currents are found. From this, the E- field outside the contour S can be found at any point and is dependent on $\hat{m}'\times\mathbf{E}(\mathbf{r}')$ and $\hat{m}'\times\nabla'\times\mathbf{E}(\mathbf{r})$ on the entire C. These are in fact proportional to the magnetic and electric surface currents, which are both unknowns. $\mathbf{E}$ is the total E- field, a superposition of the incident field and the scattered field due to the surface currents on C. For a scattering problem, the $\mathbf{E}$ (or $\mathbf{H}$) field far from the scatterer is of importance, and to find it the magnetic and electric surface currents on C must be solved. (5.10) was derived directly for the 2D case. Since the derivations in the literature were for the 3D case, another method to derive this equation was used to verify it. In this approach the 2D equations are derived directly from the 3D equations by integrating the 3D Green's functions over the infinite dimension. This confirms that the derivation of (5.10) is correct.

Stellenbosch University https://scholar.sun.ac.za

It is clear that the 2D equations can be found from the 3D equations by simply substituting the 2D free space Green's functions for the 3D Green's functions and replacing closed surface integrals by closed contour integrals. Thus the 2D Green's function is simply the 3D Green's function integrated along the infinite z-axis [24]. To solve for the electric surface current directly, (5.10) is rewritten with the use of Maxwell's curl equation as

$$\begin{aligned}\mathbf{E}(\mathbf{r}) &= \mathbf{E}_{inc}(\mathbf{r}) + \oint_C \{[\hat{n}' \times \mathbf{E}(\mathbf{r}')] \times \nabla' G_0(\mathbf{r},\mathbf{r}')) - jk_0\eta \mathbf{J}(\mathbf{r}')G_0(\mathbf{r},\mathbf{r}') \\ &- \frac{j\eta}{k_0}\nabla' \cdot \mathbf{J}(\mathbf{r}')\nabla G_0(\mathbf{r},\mathbf{r}'))\}d\ell' \end{aligned} \tag{5.11}$$

The unit vector $\hat{m}$ is now replaced with the more often used $\hat{n}$, where $\hat{n}$ from here onwards is taken as representing $\hat{m}$. Both the MFIE and EFIE (see next section) will be employed to solve for scattering from a perfectly conducting cylinder with TE or TM incidence. This will be used to decouple the BEM from the FEM and thus enabling separate testing of the codes.

5.3 Electric Field Integral Equation (EFIE)

When a perfectly conducting object is considered, the EFIE may be considered as a simplification to (5.11) and the MFIE a simplification to the dual of (5.11) in terms of the total H-field. The boundary condition is zero tangential E-field on the surface of the conductor:

$$\hat{m} \times \mathbf{E}(\mathbf{r}')|_C = 0 \tag{5.12}$$

This reduces (5.11) to

$$\mathbf{E}_{inc} = \oint_C jk\eta \mathbf{J} G_0(\mathbf{r},\mathbf{r}')d\ell' + \oint_C \frac{jk}{\eta}\nabla' \cdot \mathbf{J}\nabla G_0(\mathbf{r},\mathbf{r}')d\ell' \tag{5.13}$$

With the use of the identity $\nabla G_0(\mathbf{r},\mathbf{r}') = -\nabla' G_0(\mathbf{r},\mathbf{r}')$ and taking the cross-product with $\hat{n}$, (5.13) is

$$\begin{aligned}\hat{n} \times \mathbf{E}_{inc}(\mathbf{r}) &= \hat{n} \times \oint_C [jk\eta \mathbf{J}_s(\mathbf{r}')G_0(\mathbf{r},\mathbf{r}') \\ &+ \frac{\eta}{jk}\nabla' \cdot \mathbf{J}_s(\mathbf{r}')\nabla' G_0(\mathbf{r},\mathbf{r}')]d\ell' \quad \mathbf{r}' \text{ and } \mathbf{r} \in \mathrm{S} \end{aligned} \tag{5.14}$$

The divergence of the surface currents causes a problem when a piecewise constant approximation is used to approximate the surface current $\mathbf{J}_s$ [25]. (5.14) contains the divergence of the surface current. The resulting Dirac- delta functions at the boundary edges represent the accumulated surface charges at these positions. This degrades the accuracy of the results when the elements are very long and the positions of the accumulated charge are affected. Decreasing the length of the elements should improve the approximation.

Stellenbosch University https://scholar.sun.ac.za

5.4 Magnetic Field Integral Equation (MFIE)

The MFIE can be derived in a similar manner and is

$$\frac{1}{2}\mathbf{J} = \hat{n} \times \mathbf{H}_{inc} + \hat{n} \times \oint_C \mathbf{J}_s(\mathbf{r}') \times \nabla' G_0(\mathbf{r}, \mathbf{r}') d\ell' \tag{5.15}$$

(It is only valid for a closed surface [26, p. 255]). According to Peterson [25], the MFIE leads to more accurate results than the EFIE listed above.

5.5 Discretisation

The MFIE, EFIE and BEM equations can all be employed to solve for both TE or TM incidence. In the case of the BEM equation, the dual formulation in terms of the H- fields may also be discretised. Only vectors which lie in the cross-sectional plane (labelled the x,y plane) can be discretised (a two- dimensional implementation is considered here). This is not really a limitation. In the case of TE^z incidence, $\mathbf{E}$ and $\mathbf{J}$ is discretised, since this is contained in the x-y plane. The H -field cannot be discretised directly. For TM^z incidence, $\mathbf{H}$ and $\hat{n} \times \mathbf{E}$ must be discretised.

Consider the TE incidence case, which was chosen since the surface current varies more distinctively with changing diameters than in the case of TM incidence and is therefore a better test of the accuracy of the implementation. $\mathbf{J}$ and $\mathbf{E}$ are expanded using edge-based vector basis functions:

$$\begin{aligned} \mathbf{J} &= \sum_{k=1}^{N_S} J_k [\mathbf{S}]_k \\ \mathbf{E} &= \sum_{k=1}^{N} e_k [\mathbf{S}]_k \end{aligned} \tag{5.16}$$

Here N is the total number of basis functions and N_s the number of basis functions on the boundary C. Note that $\hat{m} \times \mathbf{E} = \hat{m} \times \sum_{k=1}^{N} e_k [\mathbf{S}]_k$ which is the magnetic surface current on contour C.

An important distinction must be pointed out: in the MFIE and EFIE case where a perfectly conducting cylinder is considered, the boundary elements are line segments and are one- dimensional simplex elements. In the FEM-BEM case, the line segments are the edges of two- dimensional simplexes (triangles). In both cases the approximation on the boundary elements can either be constant or perhaps even linear, but not of higher order with any of the 2D hierarchical basis sets described in this thesis. This is due to the fact that the order of approximation for hierarchical basis sets is increased by adding face functions inside the element which contribute normal components to the boundaries while leaving the tangential components unaffected. This is the reason why tangential components can not be of higher order than a linear approximation in the two dimensional case for hierarchical basis sets.

Stellenbosch University https://scholar.sun.ac.za

Now the surface currents are approximated as piecewise constant over each boundary element.

Here [S] is a one element matrix, since only one basis function (CT/LN) is used

$$[\mathbf{S}] = [\mathbf{w}_{ij}^{(0.5)}] \tag{5.17}$$

In the case of LT/QN approximation it would be

$$[\mathbf{S}] = [\mathbf{w}_{ij}^{(0.5)}\mathbf{w}_{ij}^{(1)}] \tag{5.18}$$

(5.11) is discretised, tested with $\hat{n} \times [\mathbf{S}_k]^T$ and integrated over C:

$$\begin{aligned}
\sum_{s=1}^{N_S} E_s \int_{C_s} (\hat{n}_s \times [\mathbf{S}_s]^T) \cdot (\hat{n}_s \times [\mathbf{S}_s]) d\ell = \sum_{s=1}^{N_S} (\hat{n}_s \times [\mathbf{S}_s]^T) \cdot (\hat{n}_s \times \mathbf{E}_{inc}) d\ell \\
+ \sum_{s=1}^{N_S}\sum_{t=1}^{N_S} E_t \int_{C_s} (\hat{n} \times [\mathbf{S}_s]^T) \cdot \hat{n}_s \times \int_{C_t} (\hat{n}_t \times [\mathbf{S}_t]) \times \nabla' G_0(\mathbf{r}, \mathbf{r}') d\ell' d\ell \\
- jk_0\eta \sum_{s=1}^{N_S}\sum_{t=1}^{N_S} J_t \int_{C_k} (\hat{n}_s \times [\mathbf{S}_s]^T) \cdot \hat{n}_s \times \int_{C_t} [\mathbf{S}_t] G_0(\mathbf{r}, \mathbf{r}') d\ell' d\ell \\
- \frac{j\eta}{k_0} \sum_{s=1}^{N_S}\sum_{t=1}^{N_S} J_t \int_{C_k} (\hat{n}_s \times [\mathbf{S}_s]^T) \cdot \hat{n}_s \times \int_{C_t} \nabla' \cdot [\mathbf{S}_t] \nabla G_0(\mathbf{r}, \mathbf{r}') d\ell' d\ell
\end{aligned} \tag{5.19}$$

(5.19) may be written as a matrix equation

$$[B][E]_c = [b] + [P][E]_c + [Q][J] \tag{5.20}$$

where the matrices are given by

$$\begin{aligned}
[B]_s^{BE} &= \int_{C_s} \hat{n}_s \times [\mathbf{S}]_s^T \cdot \hat{n}_s \times [\mathbf{S}]_s d\ell \\
[b]_s &= \int_{C_s} \hat{n}_s \times [\mathbf{S}]_s^T \cdot \hat{n}_s \times \mathbf{E}_{inc} d\ell \\
[P]_{st} &= \int_{C_s} \hat{n}_s \times [\mathbf{S}]_s^T \cdot \hat{n}_s \times \int_{C_t} \hat{n}_t \times [\mathbf{S}]_t \times \nabla G_0 d\ell' d\ell \\
[Q]_{st} &= -jk_0\eta \int_{C_s} \hat{n} \times [\mathbf{S}]_s^T \cdot \hat{n} \times \int_{C_t} ([\mathbf{S}]_t G_0 + \frac{1}{k_0^2} \nabla' \cdot [\mathbf{S}]_t \nabla G_0) d\ell' d\ell
\end{aligned} \tag{5.21}$$

and are similar, but not identical to the 3D equations presented in [2].

Stellenbosch University https://scholar.sun.ac.za

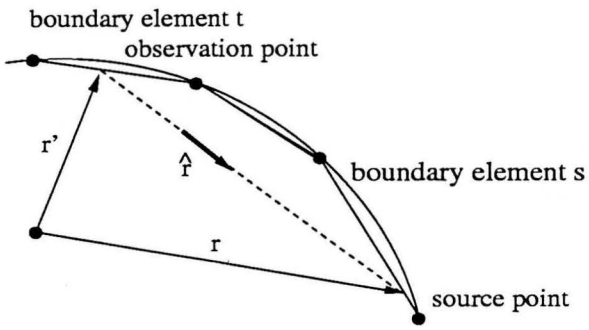

Figure 5.2: Different source and observation elements

5.6 FEM Treatment of the Interior Region

Inside the area enclosed by the contour C, a Finite Element formulation is used, with the functional to be minimised including an additional boundary contribution:

$$F(\mathbf{E}) = \frac{1}{2}\iint_S (\frac{1}{\mu_r}(\nabla \times \mathbf{E}) \cdot (\nabla \times \mathbf{E}) - k_0^2 \epsilon_r \mathbf{E} \cdot \mathbf{E}) dS$$
$$- jk\eta \oint_C \mathbf{J} \cdot \mathbf{E} d\ell \tag{5.22}$$

The minimised functional leads to the second matrix equation

$$[K][E] + [B]^{\text{FEM}}[J] = 0 \tag{5.23}$$

where

$$[B]_s^{\text{FEM}} = -jk\eta \int_{C_s} [\mathbf{S}]_s^T \cdot [\mathbf{S}]_s d\ell \tag{5.24}$$

Here, note that the $[E]$-column matrix includes the E- field coefficients on the contour itself and those of the interior region, while the $[E]_C$ column matrix that will be encountered later is only the E- field coefficients on the contour C. The boundary conditions on C links the BE and FEM equations:

$$\begin{aligned} \hat{n} \times \mathbf{E}|_{C_+} &= \hat{n} \times \mathbf{E}|_{C_-} \\ \hat{n} \times \mathbf{H}|_{C_+} &= \hat{n} \times \mathbf{H}|_{C_-} \end{aligned} \tag{5.25}$$

Now there are two matrix equations in $[E]$ and $[J]$, (5.20) and (5.23), with $[E]_c$ contained in $[E]$, allowing $[E]$ and $[J]$ to be solved. The discretisation of 5.23 is as described in chapter 1, however evaluation of the BE equations requires numerical integration and extraction of singularities which occur.

Stellenbosch University https://scholar.sun.ac.za

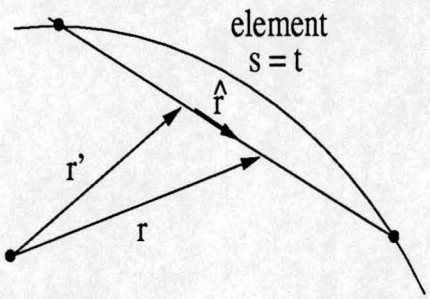

Figure 5.3: Case where source point and boundary point can be identical

5.7 Extraction of Singularities and Evaluation of Integral Equations

5.7.1 Origin of Singularities

The relevant Greens' function is

$$G_0(\mathbf{r},\mathbf{r}') = \frac{j}{4}H_0^{(2)}(k_0 R) \quad \text{where} \quad \mathrm{R} = \mid \mathbf{r} - \mathbf{r}' \mid \tag{5.26}$$

The imaginary component of the Hankel function is singular when r = 0. (5.19) involves a double integration over the contour C, on which both the source and observation points are restricted. In figures 5.2 and 5.3 the source and observation points are shown on the boundary elements. The source element is named s and the observation element is labelled t. $\hat{r}$ is defined as the unit vector from $\mathbf{r}'$ to $\mathbf{r}'$. When source and observation points are identical, r = 0. The diagonal entries of the Q and P matrices contain the contribution from the singular integrals. Analytic integration can be performed in this case to evaluate the integrals at these singular points. Table 5.1 gives the dimensions of all the matrices involved. The Hankel function can be expressed as an infinite sum and integrated analytically (Appendix B). Eventually this was found to be unnecessary, and non- coincident integration points were used.

5.7.2 Numerical Integration

Gaussian integration (10 point and 8 point) was chosen. A short introduction to Gaussian integration may be found in [27, p. 40-41], while tables with Gaussian integration formulae for various number of points are found in [28]. Appendix B shows the expressions that were integrated analytically.

5.8 Calculation of Far Fields and Scattering Width

The two matrix equations can be solved for $\mathbf{J}_s$ on the boundary C and the E- field over the interior region and on the boundary. Finally the scattering effect of the structure can be determined. The far fields must be found to do this. The same boundary equation (5.11) can be used to calculate the E- field far from the scatterer, when the sources on the boundary are known.

Stellenbosch University https://scholar.sun.ac.za

Matrix	Dimension
K	$N \times N$
B^{BE}	$N \times N_s$
B^{FEM}	$N_s \times N$
P	$N_s \times N$
Q	$N_s \times N_s$
b	$N_s \times 1$
E	$N \times 1$
J	$N_s \times 1$

Table 5.1: FEM-BEM matrix dimensions.

Consider (5.11) again:

$$\begin{aligned}\mathbf{E}(\mathbf{r}) &= \mathbf{E}_{inc}(\mathbf{r}) + \oint_C \{[\hat{m}' \times \mathbf{E}(\mathbf{r}')] \times \nabla' G_0(\mathbf{r},\mathbf{r}')) - jk_0\eta \mathbf{J}(\mathbf{r}')G_0(\mathbf{r},\mathbf{r}') \\ &- \frac{j\eta}{k_0}\nabla' \cdot \mathbf{J}(\mathbf{r}')\nabla G_0(\mathbf{r},\mathbf{r}')\} d\ell \end{aligned} \tag{5.27}$$

In a discretised form (5.27) may be used to calculate the far fields from the known surface currents. Here $\mathbf{r}$ is set to be far away from the scatterer while $\mathbf{r}'$ is found on the contour C. Each element has a contribution to the field at a point far from the scatterer.

The two dimensional radar cross sections for TE and TM incidence are defined as

$$\sigma_{2D}^{TE} = \lim_{r\to\infty} 2\pi r \left[\frac{|\, H_z^{scat}\,|^2}{|\, H_z^{inc}\,|^2}\right] \tag{5.28}$$

$$\sigma_{2D}^{TM} = \lim_{r\to\infty} 2\pi r \left[\frac{|\, E_z^{scat}\,|^2}{|\, E_z^{inc}\,|^2}\right] \tag{5.29}$$

The scattering width is the radar cross- section normalised with respect to a wavelength of 1m.

As it was chosen to work with E- fields and not H- fields, the z- directed H- field is not directly known. However the E field components are known and the z directed H field may be calculated from this, or a simpler approach could be followed. For the time harmonic case (in a sourceless region), one of Maxwell's equations is

$$\nabla \times \mathbf{H} = j\omega\epsilon\mathbf{E} \tag{5.30}$$

In cylindrical coordinates, the E field is expressed as

$$\mathbf{E} = \frac{1}{j\omega\epsilon}\left[\hat{r}\frac{1}{r}\frac{\delta H_z}{\delta\phi} - \hat{\phi}\frac{\delta H_z}{\delta r}\right] \tag{5.31}$$

In the far field the r component may be neglected, as it has a $\frac{1}{r}$ dependence. Now the scattering width is calculated using only the phi component of the E field:

Stellenbosch University https://scholar.sun.ac.za

$$\sigma_{2D}^{TE} = \lim_{r\to\infty} 2\pi r \left[\frac{|\ E_{\phi}^{scat}\ |^2}{|\ E^{inc}\ |^2}\right] \tag{5.32}$$

5.9 Conclusion

In this chapter the formulation and implementation of a method to solve a problem of infinite domain was presented. The 3D equations are found in many textbooks. It was shown that the two- dimensional scattering equations may be found simply by substituting the two- dimensional Green's function for the three- dimensional Green's function and replacing surface integrals by contour integrals. Although the E- and H- fields cannot be discretised directly, it was found that the scattering equation (5.27) may be applied for TE and TM incidence. Two integral equations which contain terms similar to (5.27), (5.15) and (5.14), were discretised and used to solve scattering from perfectly conducting cylinders.

Stellenbosch University https://scholar.sun.ac.za

Chapter 6

Applications and Results of 2D Scattering

6.1 Introduction

In chapter 5, the formulation and the construction of the matrices were discussed. All the tools are now available to investigate the application of the technique to simple and more complicated structures. To validate the code, examples where analytical solutions are available for comparison were chosen.

The MFIE and EFIE solutions of scattering from conducting cylinders were investigated to examine the effect of constant tangential components. As these terms appear in the FEM-BEM coupled technique, this proved to be very instructive. These results are also presented here.

6.2 Scattering from Perfectly Conducting Cylinders

In this case the fields are zero everywhere inside the cylinders and the only unknown is the surface current $\mathbf{J}_s$.

Solutions to the EFIE

For comparison purposes, an example from [19, p. 716], where the EFIE solution for a cylinder with radius 1 wavelength and discretisation 540 elements was presented, was chosen (figure 6.1). The ripple in the approximation which is characteristic of the EFIE solution, is also apparent in [19], although scalar basis functions were used in that case.

Stellenbosch University https://scholar.sun.ac.za

In this representation, the divergence of the surface current is the derivative of a piecewise constant approximation, which are dirac- delta functions at the element boundaries. This does not appear in the MFIE case, which explains why the EFIE solution is not as accurate. The ripple effect is also due to this approximation. However, the accuracy improves with an increase in the number of elements, although the ripple effect is not decreased. Higher order basis functions could be used to eliminate the discontinuities in the approximation, but the highest order approximation which is possible in the 2D case is a linear one. This will not remove the discontinuities between elements and the dirac- delta functions will still be present. The discontinuities were also evident in results by Peterson [9], who implemented linear tangential components.

Figure 6.1 shows the effect of a discretisation of 80 elements, to enable comparison with the MFIE solution, figure 6.3, where an 80 element discretisation (about 1/12 wavelength elements) is used. It also shows the result for a 540 element discretisation (one would never use so many elements except for a convergence investigation such as this), to enable comparison to [19, p. 716]. The scattering width calculated from the solution in figure 6.1 is shown in figure 6.2.

Solutions to the MFIE

The result for the magnetic field equation is compared to the analytic solution in figure 6.3. Good agreement is found. Much less boundary elements are necessary than in the previous case. In both cases the scattering width was calculated: figures 6.2 and 6.4.

6.3 Conclusion

Good agreement between analytic and computed results were obtained for EFIE and MFIE solutions. The reason for the ripple effect in the EFIE solution was discussed and a comparison made of EFIE solutions with a different number of boundary elements.

Stellenbosch University https://scholar.sun.ac.za

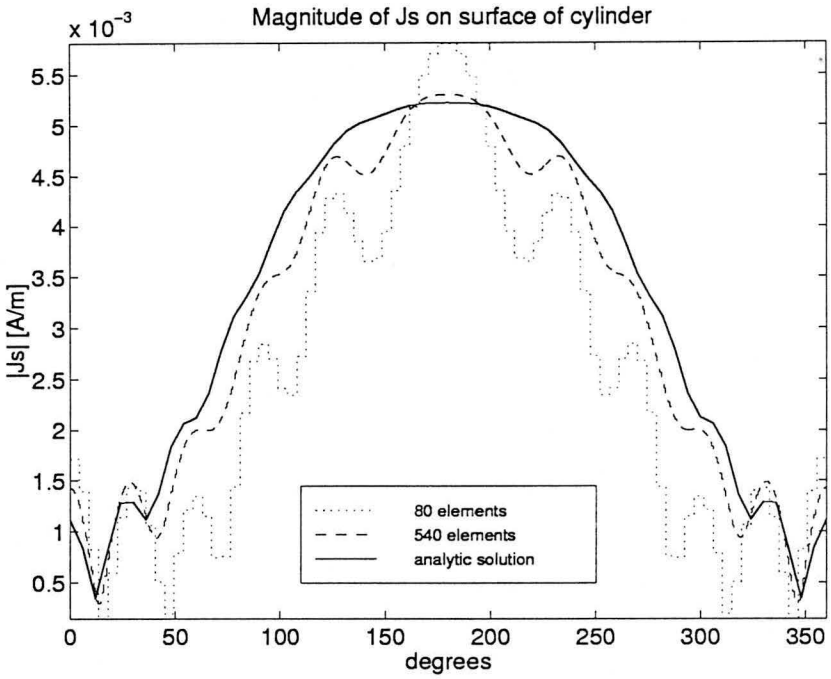

Figure 6.1: Solution for $|\mathbf{J}_s|$ on the surface of a perfectly conducting cylinder, radius 1 wavelength and infinite length, compared to the analytic solution. (Incident E field magnitude 1 V/m)

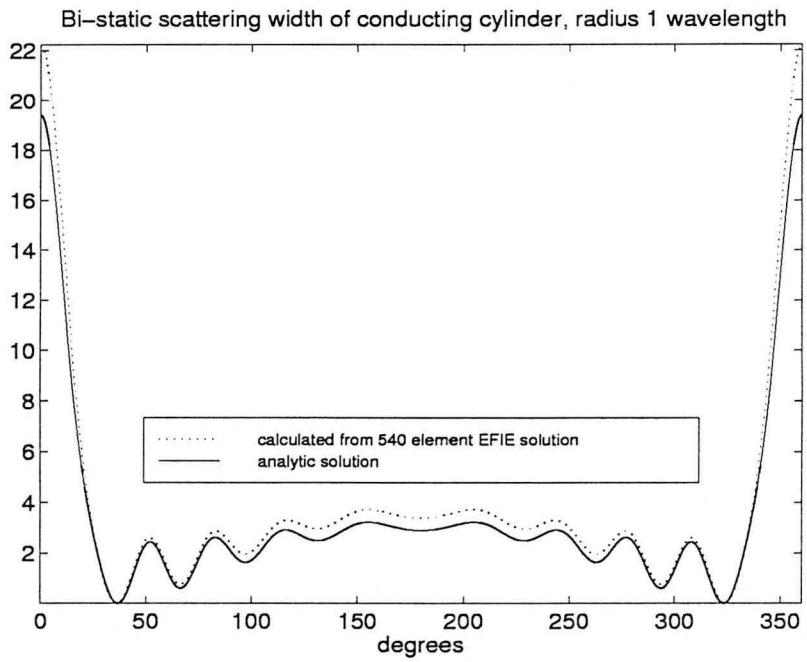

Figure 6.2: The scattering width calculated from the EFIE solution (540 elements) compared to the scattering width analytic solution. A perfectly conducting cylinder with radius 1 wavelength and infinite length was considered.

Stellenbosch University https://scholar.sun.ac.za

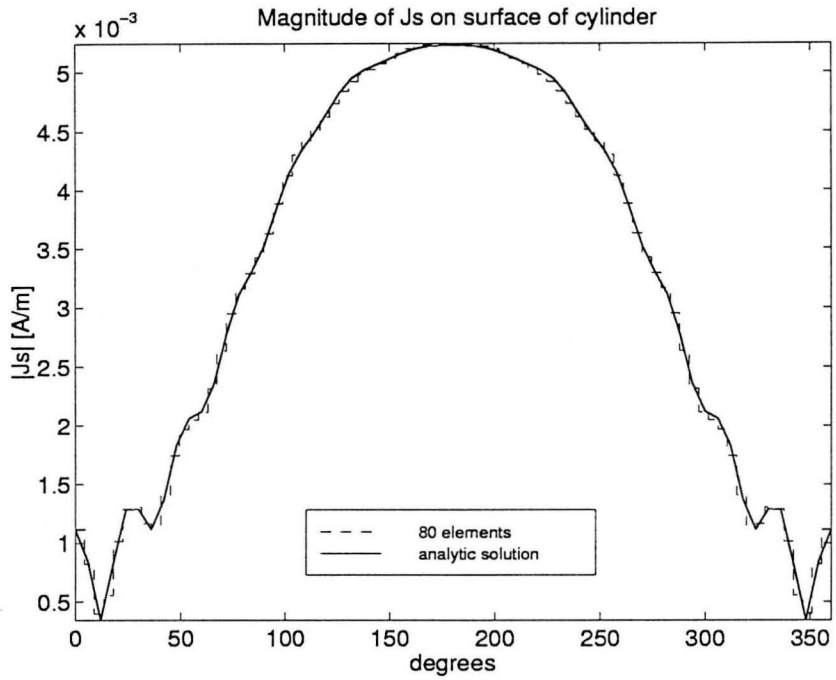

Figure 6.3: Solution for $|\ \mathbf{J}_s\ |$ on the surface of a perfectly conducting cylinder, radius 1 wavelengths and infinite length, compared to the analytic solution. (Incident E field magnitude 1 V/m, 80 boundary elements.)

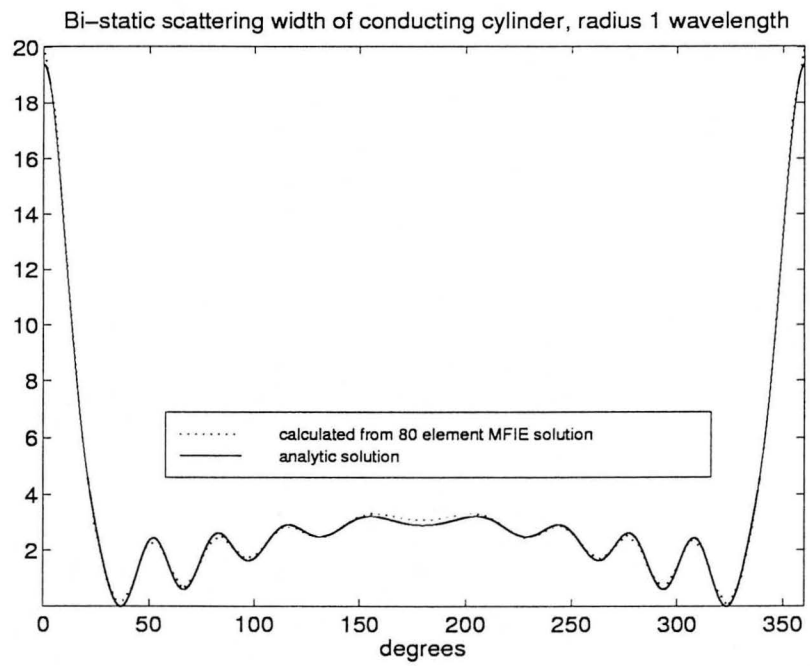

Figure 6.4: The scattering width calculated from the MFIE solution compared to the scattering width analytic solution. A perfectly conducting circular cylinder radius 1 wavelength and infinite length was considered.

Stellenbosch University https://scholar.sun.ac.za

Chapter 7

Conclusion

In this thesis only vector based finite elements were used. In the case of eigenvalue problems one of the advantages that became clear is that when used correctly, spurious modes are easily identified as those with zero eigenvalues. Continuity is enforced in a very natural manner. The results obtained were accurate and as expected confirmed the reliability of the basis sets implemented. Typical average error percentages for the TE and TM circular waveguide CT/LN wavenumbers were 0.33% and 0.6% respectively for the specific discretisation mentioned. A LT/LN approximation of the field variable was found to be inappropriate. It must be emphasised that the eigenvalues and the field values over the object cross-section were obtained in no particular order, and it is not obvious from the list of eigenvalues, which correspond to the modes of interest to the user. This was particularly noticeable in the case of the circular cross-section cylinder, which is rotationally symmetric and results in the inclusion of degenerate modes. Only when looking at the field patterns can these modes be identified. No degenerate modes were found in the case of the ridged waveguides or the dielectric cylinders with eccentric dielectric cylinders, which are not rotationally symmetric.

An extension of this work should be the application to three dimensional problems, which, except for the complication of geometry, should not require much additional effort. In this case higher order approximations than those obtained with LT/QN basis sets are not advised, as the computational times will be a restriction for larger structures. However, this depends on the computational infrastructure available.

As some difficulties were experienced with the coupling of the Finite Element Method and the Boundary Element Method at the time of writing, no comments about the accuracy of this hybrid technique can be made. Individually these techniques have been examined and provided satisfactory results as was demonstrated in chapters 4 and 6. The scattering data presented had to be limited to scattering from perfectly conducting cylinders.

On completion of the combination of the FEM-BEM, it will be possible to examine the scattering or absorbing effect of materials that can be modelled as a composition of dielectric, magnetic and perfectly conducting materials. The formulation can also handle lossy materials, although this has not been tested.

Stellenbosch University https://scholar.sun.ac.za

Appendix A

Simplex Coordinates and Simplex Elements

Simplex coordinates (also referred to as barycentric coordinates) are associated with simplex elements. Simplex elements are lines in 1D, triangles in 2D and tetrahedrons in 3D. This reveals the pattern, an N-dimensional simplex has N+1 vertices. Now simplex coordinates are defined on these elements and are entirely local within simplex elements. Figure A.1 gives an introduction to one dimensional and two dimensional simplex elements. It shows how on a line (a 1D element) only two simplex coordinates are defined, each varying linearly from the one node to the other between 0 and 1. An arbitrary point P is shown on both the 1D simplex and the 2D simplex and the expressions for the simplex coordinates are given in each case.

The advantage of simplex coordinates is that it is not necessary to consider the shape or the position of an element. Derivations are simply done for a simplex element and afterwards scaled by the area or the edge lengths, depending on where it is used. As an example, consider the following identity [2, p. 82] which is used for the calculation of the T matrix in chapter 1:

$$\oiint_{\omega_e} \lambda_1^k \lambda_2^m \lambda_3^n dx dy = \frac{2k!m!n!}{(k+m+n+2)!} A \tag{A.1}$$

A is the area of the triangle. Here the integral for any triangular element is known and scaled with the element area.

The coordinates always satisfy in N dimensions:

$$\sum_{k=1}^{N} \lambda_k = 1 \tag{A.2}$$

which imply that it is normalised.

Conversion from Cartesian coordinates to simplex coordinates is easily made by the use of

Stellenbosch University https://scholar.sun.ac.za

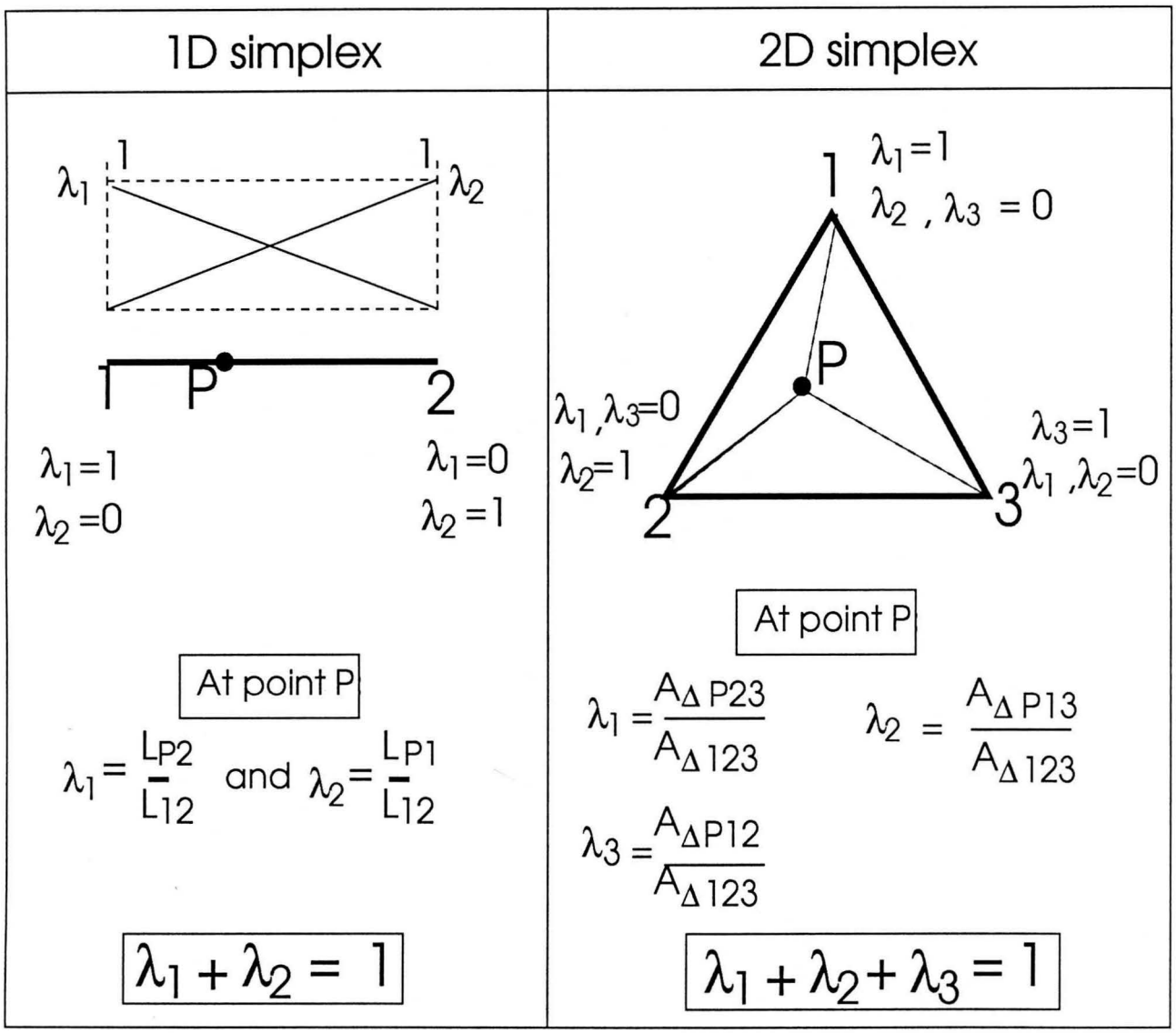

Figure A.1: The simplex elements in 1D and 2D.

$$\begin{bmatrix} \lambda_1 \\ \lambda_2 \\ \lambda_3 \end{bmatrix} = \frac{1}{2A} \begin{bmatrix} x_2y_3 - x_3y_2 & y_2 - y_3 & x_3 - x_2 \\ x_3y_1 - x_1y_3 & y_3 - y_1 & x_1 - x_3 \\ x_1y_2 - x_2y_1 & y_1 - y_2 & x_2 - x_1 \end{bmatrix} \begin{bmatrix} 1 \\ x \\ y \end{bmatrix} \tag{A.3}$$

in the 2D case, which is of interest here [1].

The gradient of a simplex coordinate $\nabla\lambda$ is often encountered and is in fact the building block for the vector basis function. A list of properties can be found in [1, p. 298], but the most important properties are illustrated in figure A.2, where $\nabla\lambda_2$ is shown: the gradient of a simplex element is a vector, which is constant over the entire element and is perpendicular to the basis opposite the vertex with which it is associated.

Some definitions and identities used often is listed below:

Stellenbosch University https://scholar.sun.ac.za

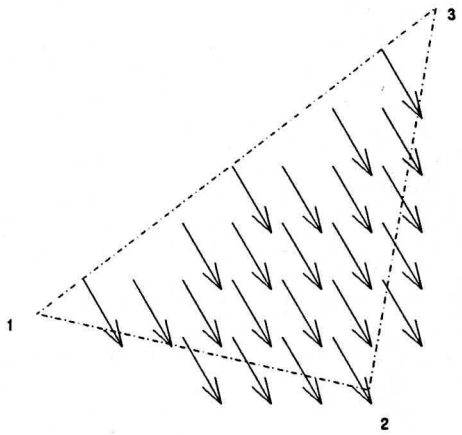

Figure A.2: The gradient of the simplex coordinate λ_2 over an entire element.

$$\begin{aligned} a_i &= x_{i+1}y_{i+2} - x_i y_{i+1} \\ b_i &= y_{i+1} - y_{i-1} \\ c_i &= x_{i-1} - x_{i+1} \end{aligned} \tag{A.4}$$

Only in 2D:

$$\nabla\lambda_i = -\frac{\hat{n}_i}{h_i} \tag{A.5}$$

Stellenbosch University https://scholar.sun.ac.za

Appendix B

Analytic Integration

This section contains the analytic integration required for the scattering equations.

The expression that contains the singularity is:

$$\oint_{C_s} \hat{m}_s \times [\mathbf{S}_s] \cdot \hat{m}_s \times \oint_{C_t} [\mathbf{S}_T]\, G_0(\mathbf{r}, \mathbf{r}') d\ell d\ell' = \int_{C_s} \int_{C_t} (\hat{m}_s \times \nabla\lambda_s) \cdot (\hat{m}_s \times \nabla\lambda_s) d\ell d\ell' \tag{B.1}$$

To write the above using simplex coordinates, the relationship $R_s\lambda_s = \ell$ and $R_t\lambda_t = \ell'$ is useful

$$R_s \cdot R_t (\hat{m}_s \times \nabla\lambda_s) \cdot (\hat{m}_s \times \nabla\lambda_t) \int_0^1 \int_0^1 G_0(\mathbf{r}, \mathbf{r}') d\ell' d\ell \tag{B.2}$$

Now let $r = \|\mathbf{r} - \mathbf{r}'\| = \mid Rel(\lambda_s - \lambda_t) \mid = \mid m \mid$, then $m = Rel(\lambda_s - \lambda_t) \mid = \mid m \mid$, then $m = R(\lambda_s - \lambda_t), dm = Rd\lambda_t$

$$R_s \cdot R_t (\hat{m}_s \times \nabla\lambda_s) \cdot (\hat{m}_s \times \nabla\lambda_t) \int_0^1 \int_{-R\lambda_s}^{R(1-\lambda_s)} G_0(k_0 \mid m \mid) dm d\lambda_s \tag{B.3}$$

This can be written as the sum of two integrals with the general form

$$\int_0^1 \int_0^{f(\lambda_s)} H_0(k_0 \mid m \mid) dm d\lambda_s \tag{B.4}$$

The function $f(\lambda_s)$ is $-R\lambda_s$ in the first case or $R(1 - \lambda_s)$. It can be shown that the contribution from these two integrations is equal in magnitude and opposite in sign and therefore the integration is done once and the result then doubled. The contribution from one of these terms will be considered.

A transformation is necessary to since the required limits of integration is from 0 to 1 (the reason for this will be clear later)

Stellenbosch University https://scholar.sun.ac.za

$$p = \frac{m}{f(\lambda_s)} \tag{B.5}$$

(B.4) is now

$$\int_0^1 \int_0^1 f(\lambda_s) H_0(k_0 \mid p f(\lambda_s) \mid) dp d\lambda_s \tag{B.6}$$

and may be split up into

$$\begin{aligned} &\int_0^1 \int_0^1 f(\lambda_s) J_0(k_0 p \mid f(\lambda_s) \mid) dp d\lambda_s \\ -j &\int_0^1 \int_0^1 f(\lambda_s) Y_0(k_0 p \mid f(\lambda_s) \mid) dp d\lambda_s \end{aligned} \tag{B.7}$$

Now the series expansion of the Bessel functions is used:

$$\begin{aligned} J_0(k_0 p \mid f(\lambda_s) \mid) &= \sum_{k=0}^{\infty} \frac{(-1)^k (k_0 f(\lambda_s) p)^{2k}}{2^{2k} (k!)^2} \\ Y_0(k_0 p \mid f(\lambda_s) \mid) &= J_0(k_0 p \mid f(\lambda_s) \mid) \left[\ln \frac{k_0 f(\lambda_s) p}{2} + \gamma \right] \\ &+ \frac{2}{\pi} \sum_{m=1}^{\infty} \frac{(-1)^{m-1} h_m}{2^{2m} (m!)^2} (k_0 f(\lambda_s) p)^{2m} \\ &= A + B \end{aligned} \tag{B.8}$$

The second term of (B.7) consists of three parts

$$\begin{aligned} &- j \int_0^1 \int_0^1 f(\lambda_s) J_0(k_0 p \mid f(\lambda_s) \mid) \ln \frac{k_0 \mid f(\lambda_s) p}{2} dp d\lambda_s \\ &- j\gamma \int_0^1 \int_0^1 f(\lambda_s) J_0(k_0 p \mid f(\lambda_s) \mid) dp d\lambda_s \\ &+ j \frac{2}{\pi} \int_0^1 \int_0^1 f(\lambda_s) \sum_{k=1}^{\infty} \frac{(-1)^{m-1} h_m}{2^{2m} (m!)^2} (k_0 p \mid f(\lambda_s) \mid)^{2k} dp d\lambda_s \\ &= I + II + III = B \end{aligned} \tag{B.9}$$

Using $\int_0^1 (\ln \lambda_s) \lambda_s^m d\lambda_s = \frac{-1}{m^2}$ and $\int_0^1 \ln p dp \approx -1$

Stellenbosch University https://scholar.sun.ac.za

$$
\begin{aligned}
A &= \gamma \sum_{k=1}^{\infty} \frac{(-1)^k (\frac{k_0 R}{2})^{2k} R}{(k!)^2 (2k+1)(2k+2)} - \frac{j\gamma R}{2} \\
I &= -j \sum_{k=0}^{\infty} \frac{(-1)^k (\frac{k_0 R}{2})^{2k}}{(k!)^2} R \left[\frac{ln(\frac{k_0 R}{2})}{(2k+1)(2k+2)} + \left[\frac{1}{(2k+2)(2k+1)^2} - \frac{1}{(2k+1)^3} \right] \right] \\
II &= -j\gamma \sum_{k=1}^{\infty} \frac{(-1)^k (\frac{k_0 R}{2})^{2k} R}{(k!)^2 (2k+1)(2k+2)} - \frac{j\gamma R}{2} \\
III &= \frac{2j}{\pi} \sum_{m=1}^{\infty} \frac{(-)^m h_m \frac{k0}{2}^{2m}}{(m!)^2 (2m+1)(2m+2)} Rel^{2m+1}
\end{aligned} \tag{B.10}
$$

The results are now added and doubled. $Q_{st} = 2K_Q(A + I + II + III)$

Now the diagonal entries of the Q matrix are calculated from this result by adding enough terms of the infinite series to ensure numerical convergence. The analytic integration is similar to that found in [29], which was used as a reference since there are similarities between the scalar and vector implementations.

Stellenbosch University https://scholar.sun.ac.za

Appendix C

Manipulation of Terms in Scattering Equations

The manipulation of expressions which are found in chapter 5 is shown here.

C.0.1 The second vector-dyadic Green's identity in 2D

A reference is made in chapter 5 to the 2D second vector-dyadic Green's identity. This could not be found in a reference for two dimensions. The derivation is a direct adaptation of the 3D derivation presented in [30, p. 70]. The surface divergence theorem is

$$\iint \nabla_s \cdot \mathbf{f} dS = \oint \hat{m} \cdot \mathbf{f} d\ell \tag{C.1}$$

where $\hat{m} = \hat{\ell} \times \hat{n}$ [23, p 299]. ∇_s is the surface divergence; it may be interchanged with the transversal del operator ∇_t since the surface has no curvature in the 2D case [30, p. 90]. Finally, the transversal del operator may interchanged with ∇, since the vector function $\mathbf{f}$ above, has no z-variation. Let $f = \mathbf{a} \times \nabla \times \mathbf{b} - \mathbf{b} \times \nabla \times \mathbf{a}$, then

$$\begin{aligned} &\iint \mathbf{b} \cdot (\nabla \times \nabla \times \mathbf{a}) - \mathbf{a} \cdot (\nabla \times \nabla \times \mathbf{b}) dS \\ &= \oint \hat{m} \cdot (\mathbf{a} \times \nabla \times \mathbf{b}) - \mathbf{b} \cdot (\hat{m} \times \nabla \times \mathbf{a}) d\ell \\ &= \oint (\hat{m} \times \mathbf{a}) \cdot (\nabla \times \mathbf{b}) + \mathbf{b} \cdot (\hat{m} \times \nabla \times \mathbf{a}) d\ell \end{aligned} \tag{C.2}$$

(C.2) is now the second 2D vector-vector Green's identity. To form the vector-dyadic identity (C.2) is simply elevated to the vector-dyadic form in the manner shown in [23, p. 10-11] and the form obtained is now

$$\begin{aligned} &\iint \{\bar{\bar{b}} \cdot (\nabla \times \nabla \times \mathbf{a}) - \mathbf{a} \cdot (\nabla \times \nabla \times \bar{\bar{b}})\} dS \\ &\oint (\hat{m} \times \mathbf{a}) \cdot (\nabla \times \bar{\bar{b}}) + (\hat{m} \times \nabla \times \mathbf{a}) \cdot \bar{\bar{b}} d\ell \end{aligned} \tag{C.3}$$

Stellenbosch University https://scholar.sun.ac.za

C.0.2 Manipulation of the scattering equation

The term $\oint_C \{\hat{m} \times \mathbf{E}(\mathbf{r}) \cdot (\nabla' \times \overline{\overline{G}}(\bar{r}', \bar{r}))d\ell'$ contains dyadic functions, which can be manipulated and rewritten in terms of vectors only.

Consider

$$\begin{aligned} \nabla' \times \overline{\overline{G}}(\bar{r}', \bar{r}) &= \nabla' \times (\overline{\overline{I}} + \frac{1}{k_0^2}\nabla\nabla)G_0(\mathbf{r}, \mathbf{r}') \\ &= \nabla' \times \overline{\overline{I}}G_0(\mathbf{r}, \mathbf{r}') + \nabla' \times (\frac{1}{k_0^2}\nabla\nabla G_0(\mathbf{r}, \mathbf{r}')) \end{aligned} \tag{C.4}$$

The second part is found to be zero so that $\nabla' \times \overline{\overline{G}}(\bar{r}', \bar{r}) = \nabla' \times \overline{\overline{I}}G_0(\mathbf{r}, \mathbf{r}')$.

Then

$$\begin{aligned} & \oint_C \hat{n} \times \mathbf{E}(\mathbf{r}) \cdot (\nabla' \times \overline{\overline{G}}(\bar{r}', \bar{r}))d\ell' \\ = & \oint_C \hat{n} \times \mathbf{E}(\mathbf{r}) \cdot \nabla' \times \overline{\overline{I}}G_0(\mathbf{r}, \mathbf{r}')d\ell' \\ = & \oint_C \hat{n} \times \mathbf{E}(\mathbf{r}) \cdot \nabla' G_0(\mathbf{r}, \mathbf{r}') \times \overline{\overline{I}}d\ell' \\ = & \oint_C \hat{n} \times \mathbf{E}(\mathbf{r}) \times \nabla G_0(\mathbf{r}, \mathbf{r}')d\ell' \end{aligned} \tag{C.5}$$

where the identity

$$\mathbf{A} \cdot (\nabla G \times \overline{\overline{I}}) = (\mathbf{A} \times \nabla G) \cdot \overline{\overline{I}} = \mathbf{A} \times \nabla G \tag{C.6}$$

has been used.

Stellenbosch University https://scholar.sun.ac.za

Appendix D

Mesh Generation

It is not a trivial problem to generate meshes with desirable properties, and numerous publications on this topic are available. While a region may be meshed with uniform elements, this is not always possible or desirable. Often Delaunay mesh generators are used.

D.1 Delaunay Triangulation

D.1.1 Definition

The Delaunay tessellation is defined in terms of its dual, the Voronoi tessellation. Given a set of points in a plane, the Voronoi tessellation consists of contiguous tiles, each tile containing all the points closest to the defining point of that tile. A more formal and exact statement of this is the definition 1 in [31]. Now the Delaunay tessellation is the connected triangles formed by connecting points in adjacent tiles.

D.1.2 Properties

Empty Circumcircle Property

Three given points in a plane uniquely define a circle through these points. The centre of this circumcircle is the intersection of the perpendicular bisector of each side of the triangle formed by connecting the three points.

A Delaunay triangulation leads to the circumcircle of each triangle to be empty, i.e. no vertices of other triangles may be found inside or on the perimeter of the circumcircle. This test is used when tessellations are constructed to verify that the mesh satisfies the definition.

Maximising Minimum Angles

It can be proved that a Delaunay triangulation guarantees that the minimum angle formed by the triangulation is maximised [31]. Similarly the maximum angle is minimised.

Stellenbosch University https://scholar.sun.ac.za

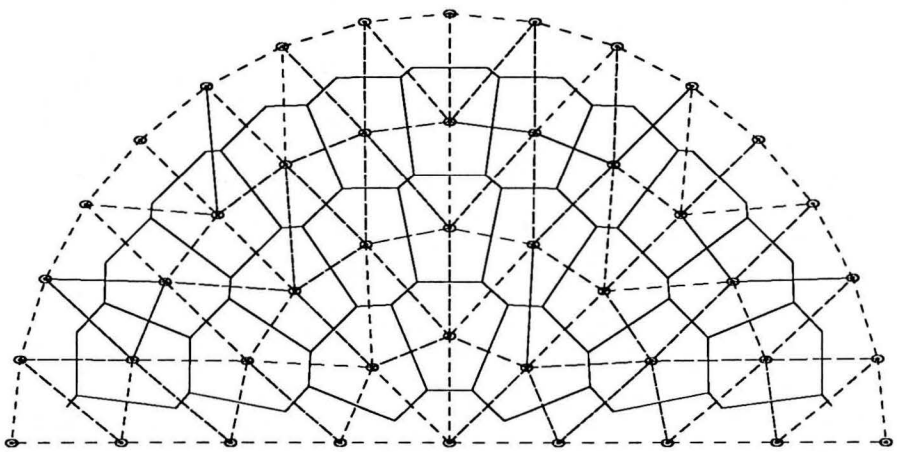

Figure D.1: Delaunay and Voronoi tessellation indicated for nodes representing half of a circular waveguide cross section.

Stellenbosch University https://scholar.sun.ac.za

Bibliography

[1] P. P. Silvester and R. L. Ferrari, *Finite Elements for Electrical Engineers*, Cambridge University Press, Cambridge, 3rd edition, 1996.

[2] J. Jin, *The Finite Element method in electromagnectics*, John Wiley and Sons, New York, 1993.

[3] Jin-Fa Lee and Raj Mittra, "A note on the application of edge-elements for modeling three-dimensional inhomogeneously-filled cavities," *IEEE Trans. Microwave Theory Tech.*, vol. 40, no. 9, pp. 1767–1773, September 1992.

[4] J. P. Webb and B. Forghani, "Hierarchal scalar and vector tetrahedra," *IEEE Trans. Magn.*, vol. 29, no. 2, pp. 1495–1498, March 1993.

[5] J. S. Savage and A. F. Peterson, "Higher order vector finite elements for tetrahedral cells," *IEEE Trans. Microwave Theory Tech.*, vol. 44, no. 6, pp. 874–879, June 1996.

[6] J.S. Savage, "Comparing high order vector basis functions," in *Proceedings of the 9th Annual Review of Progress in Applied Computational Electromagnetics*, March 1998, pp. 742–749, Held in Monterey, CA.

[7] D. Sun, J. Manges, X. Yuan, and Z. Cendes, "Spurious modes in Finite Element methods," *IEEE Ant. Prop. Magazine*, vol. 37, no. 5, pp. 12–24, October 1995.

[8] P. P. Silvester and G. (ed) Pelosi, *Finite Elements for wave electromagnetics, methods and techniques*, IEEE Press, New York, 1992.

[9] A. F. Peterson, "Vector finite element formulation for scattering from two-dimensional heterogeneous bodies," *IEEE Trans. Antennas Propagat.*, vol. 43, no. 3, pp. 357–365, March 1994.

[10] Z. J. Cendes, "Vector finite elements for electromagnetic field computation," *IEEE Trans. Magn.*, vol. 27, no. 5, pp. 3958–3966, September 1991.

[11] J. C. Nedelec, "Mixed finite elements in $\mathcal{R}^3$," *Numerische Mathematik*, vol. 35, pp. 315–341, 1980.

[12] J. P. Webb, "Edge elements and what they can do for you," *IEEE Trans. Magn.*, vol. 29, no. 2, pp. 1460–1465, March 1993.

[13] A. Ahagon and T. Kashimoto, "Three-dimensional electromagnetic wave analysis using high order edge elements," *IEEE Trans. Magn.*, vol. 31, no. 3, pp. 1753–1756, May 1995.

Stellenbosch University https://scholar.sun.ac.za

[15] J. C. Nedelec, "A new family of mixed finite elements in $\mathcal{R}^3$," *Numerische Mathematik*, vol. 50, pp. 57–81, 1986.

[16] D. C. Dibben and R. Metaxis, "A comparison of the errors obtained with Whitney and linear edge elements," *IEEE Trans. Magn.*, vol. 33, no. 2, pp. 1524–1527, March 1997.

[17] R. H. Hansmann and D. B. Davidson, "Two dimensional edge-based finite elements for guided and scattered wave problems," in *Proceedings of the 1998 COMSIG Symposium*, September 1998, pp. 415–418, Held at UCT, Cape Town, South Africa.

[18] S. Ramo, J. R. Whinnery, and T. van Duzer, *Fields and Waves in Communication Electronics*, John Wiley and Sons, 3rd edition, 1994.

[19] C. A. Balanis, *Advanced Engineering Electromagnetics*, John Wiley and Sons, New York, 1989.

[20] J. R. Pyle, "The cutoff wavelength of the TE_{10} mode in ridged rectangular wavguide of any aspect ratio," *IEEE Trans. Microwave Theory and Techniques*, vol. MTT-14, no. 4, pp. 175–183, April 1966.

[21] J.-M. Jin, J. L. Volakis, and J. D. Collins, "A Finite Element -Boundary Integral method for scattering and radiation by two- and three- dimensional structures," *IEEE Trans. Antennas Mag.*, vol. 33, no. 3, pp. 22–32, June 1991.

[22] J. A. Kong, *Electromagnetic Wave Theory*, John Wiley and Sons, New York, 1986.

[23] C. T. Tai, *Dyadic Green's Functions in Electromagnetic Theory*, Intext Educational Publishers, Scranton, 1971.

[24] I. V. Lindel, *Methods for electromagnetic field analysis*, Clerendon Press, Oxford, 1992.

[25] A. F. Peterson, "Analysis of heterogeneous electromagmetic scatterers: Research progress of the past decade," *IEEE Proc.*, vol. 44, no. 6, pp. 1431–1441, June 1991.

[26] P. P. Silvester and R. L. Ferrari, *Finite Elements for Electrical Engineers*, Cambridge University Press, Cambridge, 2nd edition, 1990.

[27] C. A Brebbia (ed), *Topics in boundary element research, volume 3*, Springer-Verlag, Berlin, 1987.

[28] M. Abramowitz and I. A. Stegun, Eds., *Handbook of Mathematical Functions*, Dover, New York, 1972.

Stellenbosch University https://scholar.sun.ac.za

[29] F.J.C. Meyer, *Hybrid Finite Element/Boundary Element solutions of general two dimensional electromagnetic scattering problems (M.Eng thesis)*, US, Stellenbosch, 1991.

[30] C-T. Tai, *Generalized vector and dyadic analysis*, IEEE Press, New York, 1992.

[31] L Guibas and J. Stolfi, "Primitives for the manipulation of general subdivisions and the computation of Voronoi diagrams," *ACM Transactions on Graphics*, vol. 4, 1985.

[32] D. B. Davidson and R. H. Hansmann, "Higher- order 2d and 3d vector Finite Elements for electromagnetic wave eigenvalue problems," in *Proceedings of the Annual Review of Progress in Applied Computational Electromagnetics*, Accepted for publication 1999.